

Cover Page



Universiteit Leiden



The handle <http://hdl.handle.net/1887/138670> holds various files of this Leiden University dissertation.

**Author:** Gagestein, B.

**Title:** Chemical tools to study lipid signaling

**Issue Date:** 2020-12-16

## Chapter 6

# Profiling the anandamide reuptake inhibitor WOBE437\*

### Introduction

Anandamide (AEA) is a lipid signaling molecule that belongs to the endocannabinoid system (ECS). It modulates neurotransmitter release via activation of the cannabinoid CB1 receptor (CB1R).<sup>1</sup> AEA is produced by hydrolysis of phospholipids, mainly by *N*-acylphosphatidylethanolamine phospholipase D (NAPE-PLD), after which it is released to activate the CB1R. AEA-induced CB1R signaling is terminated by a two-step process, i.e. cellular uptake and hydrolysis of the amide bond by fatty acid amide hydrolase (FAAH). The ECS is responsible for regulation of a large number of physiological processes, including energy balance, pain, inflammation and neurotransmission.<sup>2</sup> Consequently, modulation of ECS signaling may have therapeutic benefits for a number of diseases, including neurodegenerative,<sup>3,4</sup> inflammatory<sup>5</sup> and cardiovascular diseases,<sup>6–8</sup> pain,<sup>9,10</sup> psychiatric disorders,<sup>2,11</sup> obesity,<sup>12</sup> and others.<sup>13</sup> Activation of CB1R signaling has been achieved by direct and indirect methods, through the application of CB1R agonists and through altering endocannabinoid metabolism, respectively.<sup>13</sup> The latter strategy may lead to fewer side effects that are usually associated with direct CB1R activation.<sup>14</sup>

---

\*The data presented in this chapter was gathered in collaboration with Floor Stevens, Domenico Fazio, Bogdan I. Florea, Alexander Bakker, Hans den Dulk, Kim Wals, Aron Smids, Herman S. Overkleeft, Mauro Maccarrone, Mario van der Stelt.

Elevation of AEA levels can be achieved by inhibiting its cellular reuptake, or by inhibiting FAAH. While inhibition of FAAH is well-characterized and selective inhibitors are currently tested in phase 2 clinical trials, the mechanism of AEA reuptake remains unclear. Small lipophilic molecules may diffuse freely through the lipid bilayer, but AEA reuptake can be saturated.<sup>15</sup> This indicates that a protein facilitator for transport across the membrane may exist. Numerous candidates for a purported endocannabinoid membrane transporter and their inhibitors (AM404,<sup>16</sup> VDM11,<sup>17</sup> UCM707,<sup>18</sup> OMDM-1/2<sup>19</sup>) have been reported, but the existence of such a transporter remains subject of intense scientific debate.<sup>20–25</sup> One of the difficulties encountered in the field is the technical challenge of reliably measuring AEA uptake in short timeframes.<sup>24</sup> Moreover, FAAH inhibition results in an intracellular accumulation of AEA, which disrupts the concentration gradient across the cellular membrane that normally drives AEA uptake.<sup>25</sup> Consequently, many AEA uptake inhibitors have been revealed to act through inhibition of FAAH.<sup>25,26</sup> Another confounding factor is inhibition of intracellular transport of AEA, which can also reduce AEA reuptake. For example, inhibition of FABP5, which is an intracellular binding protein that transports AEA to FAAH at the endoplasmic reticulum,<sup>27</sup> blocks AEA uptake.<sup>28</sup> Other intracellular AEA binding proteins are Hsp70,<sup>29</sup> albumin and potentially FLAT, a catalytically inactive version of FAAH.<sup>30</sup>

Recently, WOBE437 (**1**, Figure 1) has been reported by Dr. Gertsch and co-workers as a novel, natural product-based AEA uptake inhibitor, which is selective over FAAH, FABP5, Hsp70, and FLAT.<sup>31</sup> WOBE437 reduced AEA uptake in mouse neuroblastoma Neuro-2a cells and in primary neurons in a concentration-dependent manner. In BALB/c mice, WOBE437 was orally bioavailable and induced CB1R-dependent anxiolytic, anti-inflammatory and analgesic effects.<sup>32</sup> Absence of FAAH inhibition was demonstrated in different assay systems, including recombinant FAAH, cell lysates and brain homogenates. Moreover, WOBE437 retained activity in FAAH-deficient HMC-1 human mast cells.<sup>33</sup> Although its pharmacological properties have been well-studied, the identity of its primary target remains unknown.

To identify targets of WOBE437, photoaffinity-based protein profiling (AfbPP) may be of use.<sup>34</sup> AfbPP makes use of bifunctional photoaffinity probes, which consist of a ligand of interest functionalized with a photoreactive group and a bioorthogonal ligation handle. After administration of the probe to intact cells, the photoreactive group is activated by UV light. This results in the formation of a reactive intermediate that may form a covalent bond with amino acids that interact with the probe. An alkyne group in the probe serves as a ligation handle to introduce reporter groups by copper(I)-catalyzed azide-alkyne cycloaddition (CuAAC) chemistry. A fluorophore-azide can be conjugated to visualize interacting proteins by sodium dodecyl sulfate polyacrylamide gel electrophoresis (SDS-PAGE) and fluorescence scanning, or alternatively, a biotin-azide can be ligated for protein isolation and identification using liquid chromatography-mass spectrometry (LC-MS).<sup>35</sup> Previously, a photoactivatable WOBE437 derivative was reported.<sup>31</sup> This derivative, RX-055 (**2**, Figure 1), showed similar activity to WOBE437 and retained activity after UV-irradiation in washout experiments, whereas

WOBE437 did not. This indicated that WOBE437 binds reversibly to a protein target, which can be irreversibly blocked by RX-055. However, as this probe only contains a photoreactive group, it cannot be used in AfBPP experiments to identify the targeted proteins. Therefore, the aim of the current study was to develop an alternative photoaffinity-based probe (pac)-WOBE (**3**) to map the protein interaction landscape of WOBE437 (Figure 1).

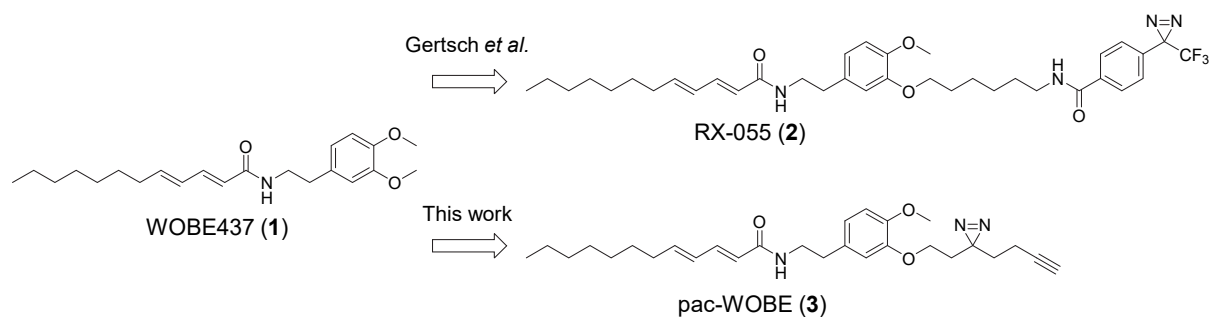


**Figure 1 | Structures of WOBE437 and its probe derivatives.**

## Results

### WOBE437 increases anandamide uptake by disrupting NAE levels

First, WOBE437 was synthesized according to previously reported procedure (Figure 2A).<sup>31</sup> A Horner–Wadsworth–Emmons reaction with (*E*)-dec-2-enal (**4**) and ethyl 2-(diethoxyphosphoryl)acetate resulted in ester **5**, which was saponified to afford carboxylic acid **6**. A subsequent peptide coupling with 2-(3,4-dimethoxyphenyl)ethan-1-amine gave WOBE437 in 49% yield over three steps. The compound was characterized in a [<sup>3</sup>H]-AEA uptake assay in Neuro-2a cells following a previously published method.<sup>36</sup> In brief, Neuro-2a cells were treated with vehicle, WOBE437 or positive control OMDM-1 for 10 min in serum-free medium, which was replaced with PBS containing AEA (400 nM) spiked with [<sup>3</sup>H]AEA. After 15 min, the cells were thoroughly washed and resuspended in aq. NaOH for measurement in a scintillation counter. Passive uptake at 4 °C was subtracted and uptake of OMDM-1-treated cells was set as baseline. In contrast to previous reports,<sup>31</sup> WOBE437 resulted in a concentration-dependent increase in uptake of anandamide when compared to the positive control OMDM-1 (Figure 2B).

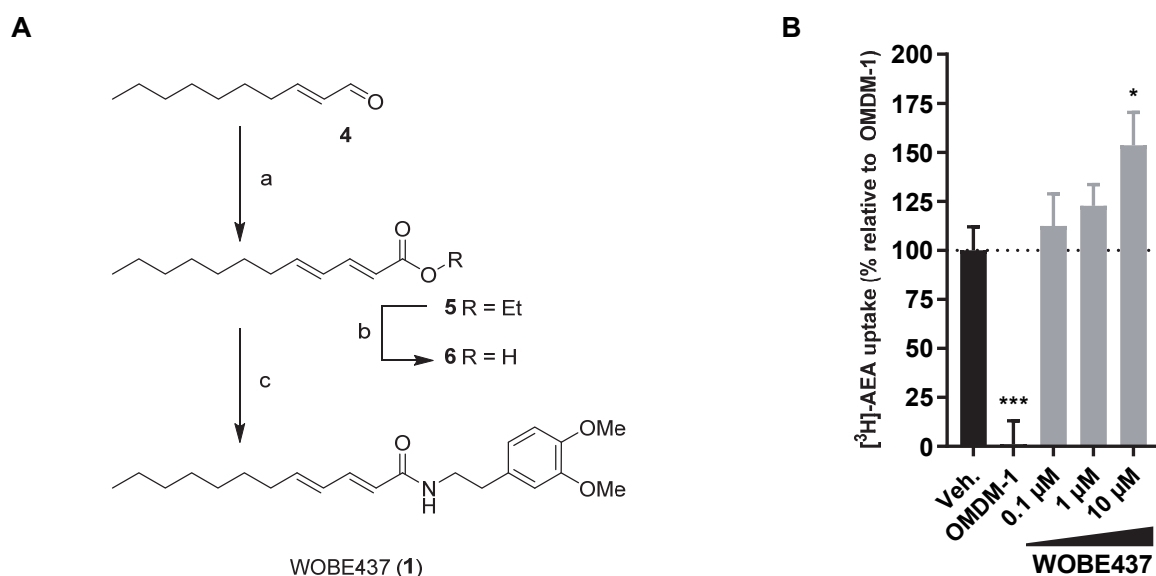


**Figure 2 | Synthesis and characterization of WOBE437. (A)** Reagents and conditions: (a) Ethyl 2-(diethoxyphosphoryl)acetate, NaH, 0 °C, then (*E*)-dec-2-enal, -78 °C to rt, 63%; (b) NaOH, 60 °C, quant.; (c) 2-(3,4-dimethoxyphenyl)ethan-1-amine, HOAt, EDC, rt, 78%. **(B)** Endocannabinoid uptake was assayed in Neuro-2a cells, which were preincubated with OMDM-1 (40 μM) as a positive control or different concentrations of WOBE437 for 10 min. [<sup>3</sup>H]-AEA was added and cells were incubated for an additional 15 min, washed and harvested to measure radioactivity. Control experiments were also carried out under the same conditions at 4 °C in order to subtract passive diffusion from active uptake. Data are expressed as means ± SEM of three independent experiments, each performed in triplicate. \* *p* < 0.05; \*\*\* *p* < 0.001 in comparison to vehicle-treated control (Dotted line) using a one-way ANOVA with Dunnett's multiple comparisons correction.

To investigate the cellular effects of WOBE437 in more detail, *N*-acylethanolamines (NAEs), free fatty acids and monoacylglycerides were measured using a LC-MS-based assay (Table S2). Neuro-2a cells were incubated for different time periods with either WOBE437 or vehicle, washed and lipids were extracted. Compared to vehicle-treated Neuro-2a cells,

WOBE437 induced a time-dependent decrease in all NAE levels, except SEA, PDEA and DHEA (Figure 3, Figure S1). The largest decrease was observed after 30 min. No effect on free fatty acids or monoacylglycerols was found (Figure S2C). Previously, the inhibition of AEA uptake by WOBE437 was shown to be dependent on the passage number of Neuro-2a cells, but no effect of passage number was found in the current study (Figure S2A, B).

The decrease in NAE levels is consisted with increased AEA uptake, as the transport is driven by the concentration gradient across the plasma membrane.<sup>21</sup> To investigate whether the reduction of NAEs was due to inhibition of NAPE-PLD, WOBE437 was tested in a surrogate substrate-based fluorescence assay using purified enzyme (Figure S3A). WOBE437 did not inhibit NAPE-PLD activity, nor was any serine hydrolase inhibited as indicated by activity-based protein profiling (Figure S3B).<sup>37</sup>

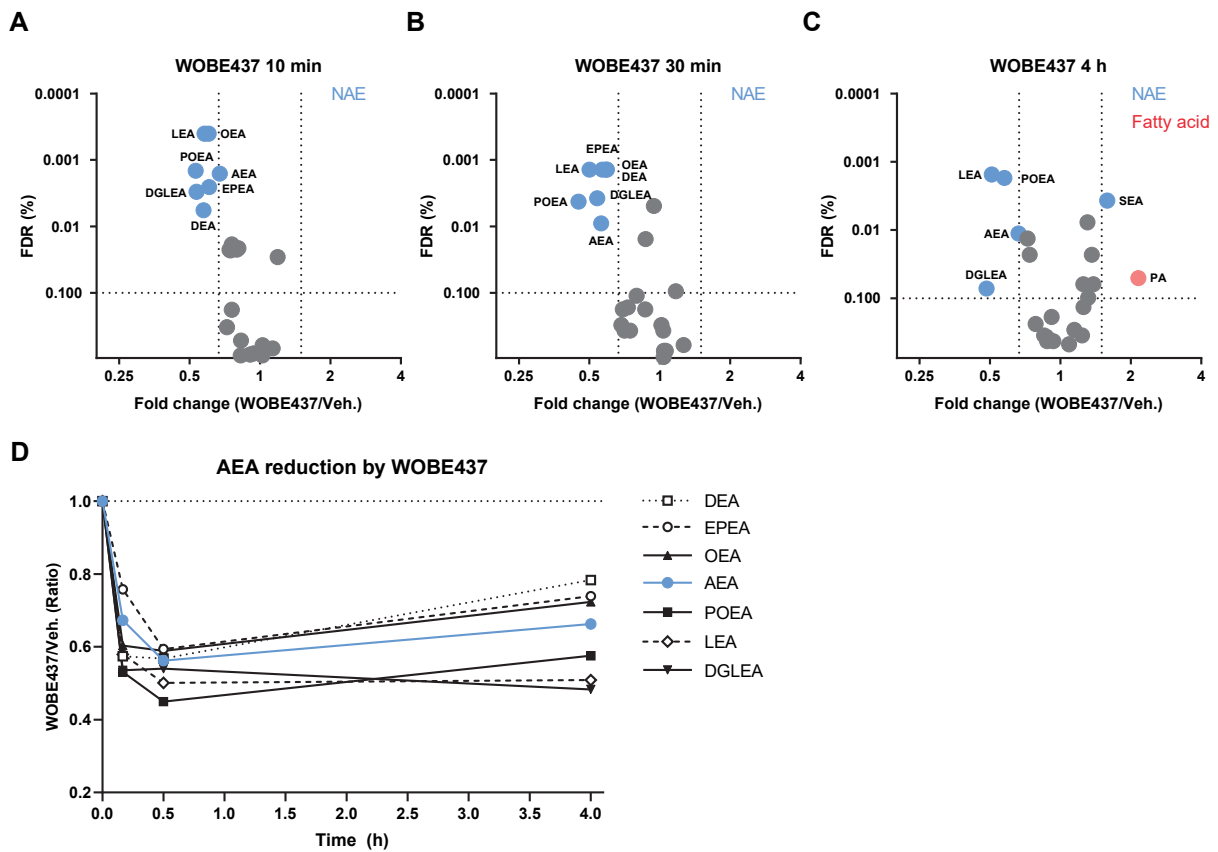


**Figure 3 | WOBE437 disrupts NAEs within 10 minutes of treatment.** Neuro-2a cells were treated with 10  $\mu$ M WOBE437 or vehicle and harvested at the indicated time points to be analyzed by MS-based lipidomics. **(A, B, C)** Lipidomic data are presented as a volcano plot and lipids with a fold-change threshold of  $\geq 1.50$  or  $\leq 0.67$  and a Benjamini-Hochberg false-discovery rate (FDR)  $\leq 10\%$  following a Student's t-test are represented by colored circles indicating lipid class. **(D)** Fold-change of altered NAEs are represented as a function of time. The complete list of ratios at 30 min are depicted in Figure S1.

## Synthesis and characterization of pac-WOBE (3)

To profile the protein interaction landscape of WOBE437, a photoaffinity probe (**3**) was designed, guided by the reported structure-activity relationship.<sup>31</sup> A minimalist diazirine and alkyne-containing moiety<sup>38</sup> was introduced on the phenyl ring of WOBE437 by peptide coupling 5-(2-aminoethyl)-2-methoxyphenol with **6** after which an S<sub>N</sub>2 substitution on 3-(but-3-yn-1-yl)-3-(2-iodoethyl)-3*H*-diazirine afforded pac-WOBE (**3**) in 12% yield over 2 steps (Figure 4A).

To visualize the protein targets of WOBE437 by gel-based AfBPP, Neuro-2a cells were incubated with **3** and irradiated with UV light (350 nm, 10 min, "UV") or exposed to ambient light ("no UV"). The cells were harvested, lysed and the probe-bound proteins were conjugated to Cy5-N<sub>3</sub> under CuAAC conditions. The protein samples were resolved by SDS-PAGE and visualized by in-gel fluorescence scanning (Figure 4B). This showed that **3** could UV-dependently label several proteins. Pretreatment of the cells with WOBE437 resulted in a reduced labeling intensity of two bands around 50 kDa, which suggested that these proteins specifically interact with WOBE437.

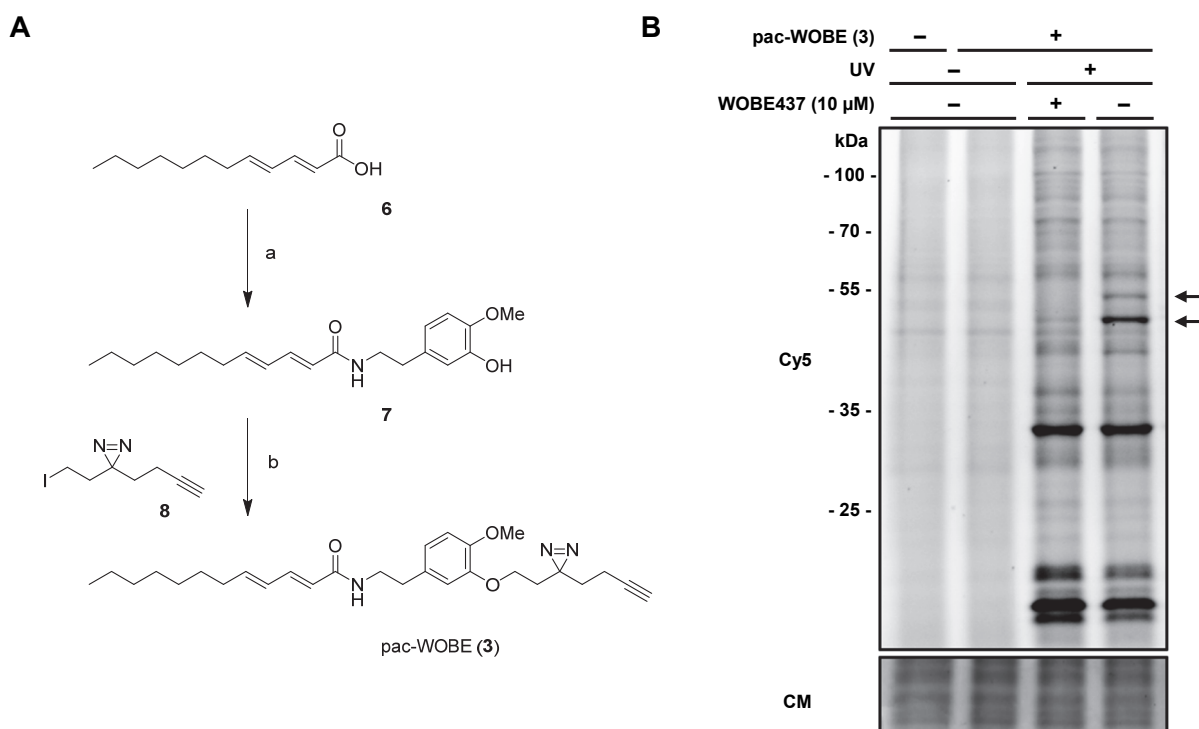


**Figure 4 | Synthesis and characterization of pac-WOBE (3).** **(A)** Reagents and conditions: (a) 5-(2-aminoethyl)-2-methoxyphenol, HOBt, EDC, 0 °C to rt, 43%; (b) 3-(but-3-yn-1-yl)-3-(2-iodoethyl)-3*H*-diazirine, K<sub>2</sub>CO<sub>3</sub>, 60 °C, 29%. **(B)** Neuro-2a cells were treated with 10 μM WOBE437 or vehicle and subsequently with 0.1 μM pac-WOBE (**3**) or vehicle, irradiated, lysed and proteomes were conjugated to Cy5-N<sub>3</sub> using CuAAC chemistry and analyzed by SDS-PAGE and in-gel fluorescence scanning. Coomassie served as a protein loading control. Arrows indicate WOBE437-competeted targets.

## Identification and characterization of WOBE437 targets

Next, a label-free chemical proteomics experiment was performed to identify the WOBE437-interacting proteins.<sup>39</sup> Neuro-2a cells were pretreated with WOBE437 (10  $\mu$ M) or vehicle, after which they were incubated with 1.0 or 0.1  $\mu$ M pac-WOBE (**3**) with or without UV exposure. Cells were lysed and treated with biotin-N<sub>3</sub> under CuAAC conditions. Probe-bound proteins were enriched using avidin-coated agarose beads, digested by trypsin and analyzed by LC-MS/MS. Proteins displaying >2-fold UV enrichment with a p-value <0.05 were designated as pac-WOBE-interacting targets. This afforded 39 and 8 significantly UV-enriched targets for the two probe concentrations, respectively (Figure 5A, S4A, Table S4). Three of these probe targets (i.e. Saccharopine dehydrogenase-like oxidoreductase (SCCPDH), Vesicle Amine Transport 1 (VAT1) and Ferrochelatase (FECH)) could be outcompeted by preincubation with WOBE437 (Figure 5B, S4A, Table S4).

Mouse and human orthologues of these three targets were recombinantly expressed in HEK-293-T cells and target engagement with AEA was investigated using gel-based AfBPP (Figure 5C, D). AEA engaged in a dose-dependent manner with SCCPDH and VAT1. Of note, AEA binding was most potent on the mouse orthologue of SCCPDH (Figure 5D, E). AEA did not compete with pac-WOBE (**3**) labeling of FECH, a mitochondrial enzyme extensively studied for its role in heme biosynthesis, and a common off-target of kinase inhibitors<sup>40</sup> and lipid probes.<sup>41</sup>

In view of these results, further experiments were conducted with mouse SCCPDH and mouse VAT1. VAT1 has previously been shown to be involved in lipid binding and transport.<sup>42,43</sup> To investigate whether SCCPDH and VAT1 were selective for WOBE437 and AEA, competitive AfBPP was performed with a selection of other closely related lipids, such as 2-arachidonoylglycerol (2-AG), palmitoylethanolamide (PEA), arachidonic acid (AA), and the FAAH inhibitor URB597 (Figure 5F-I). WOBE437 was the most potent competitor of mSCCPDH labeling followed by AEA > URB597 > AA > 2-AG > PEA. Mouse VAT1 was much more selective since its labeling was only significantly inhibited by WOBE437, AEA and PEA (Figure 5G-I).

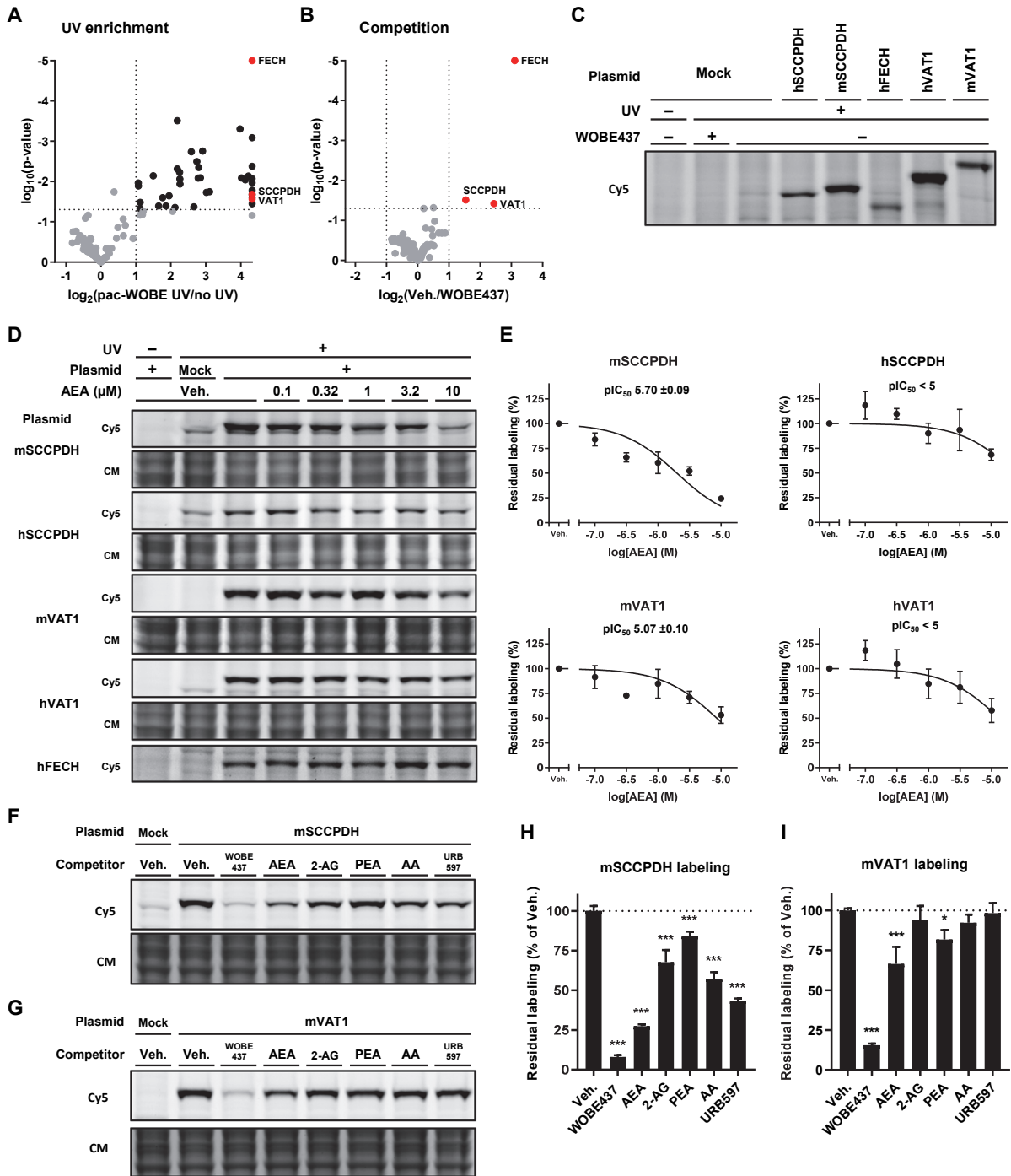
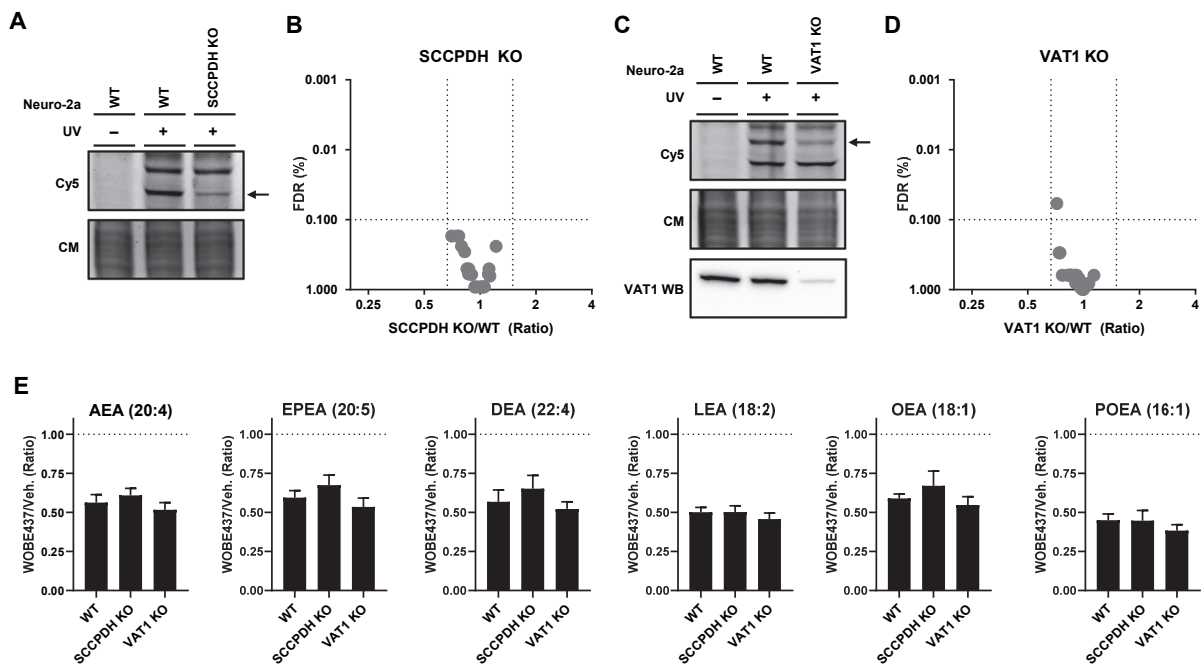


**Figure 5 | Identification and characterization of WOBE437 targets using pac-WOBE (3).** Volcano plot depicting (A) UV enrichment and (B) WOBE437 competition of proteins labeled by *in situ* AFBPP in Neuro-2a cells using 1 μM pac-WOBE (3). UV enrichment is capped at 20-fold, p-value at 0.00001. A complete list of targets are listed in Table S4. (C) Gel-based AFBPP profiling of overexpressing HEK-293-T cells using 0.1 μM pac-WOBE (3). (D) Representative gels of AEA competition of 0.1 μM pac-WOBE (3) labeling of overexpressing HEK-293-T cells. (E) Quantified residual labeling of indicated protein by 0.1 μM pac-WOBE (3) after AEA preincubation. Fluorescent signal was quantified, corrected by Coomassie and expressed as remaining labeling compared to vehicle. Data represent means ± SD of three separate experiments and  $pIC_{50} \pm SD$ . (F, G) Representative gels of competition of 0.1 μM pac-WOBE (3) labeling of overexpressing HEK-293-T cells. (H, I) Quantified residual labeling of indicated protein by 0.1 μM pac-WOBE (3) after preincubation with indicated compound. Data represent means ± SD of three biological replicates. \*  $p < 0.05$ , \*\*\*  $p < 0.001$  in comparison to vehicle-treated control (dotted line) using a one-way ANOVA with Dunnett’s multiple comparisons correction.

Next, a genetic approach was used to investigate whether SCCPDH or VAT1 is responsible for WOBE437-induced decrease in NAE levels in Neuro-2a cells, since no selective SCCPDH or VAT1 inhibitors are available. Of note, single cell heterogeneity in NAE production prevented the unequivocal analysis of single cell clone knockouts.<sup>44</sup> Therefore, disruption of SCCPDH and VAT1 genes was performed by three sequential rounds of transfection of Cas9 and single guide RNAs (sgRNA) in Neuro-2a cell populations. SCCPDH and VAT1 expression in these cell populations was significantly, albeit not completely, decreased as determined by gel-based AfBPP and western blot for VAT1 (Figure 6A, C). The residual expression of SCCPDH and VAT1 can be explained by a transfection efficiency below 100% and by insertion or deletion of a full codon upon Cas9-mediated DNA modification, thus preventing the frameshift that generally results in an early STOP-codon. Next, the cellular NAE levels of these genetically modified Neuro-2a populations were determined using LC-MS and serine hydrolase activity by ABPP. No change in NAE levels or serine hydrolase activity was observed for these knockdown populations compared to wild type cells (Figure 6B, D and Figure S5, S6). Notably, WOBE437 was still able to significantly reduce NAE levels in these genetically modified cells (Figure 6E). This indicated that other targets than SCCPDH or VAT1 are responsible for the WOBE437-mediated reduction in NAE levels.



## Conclusion

WOBE437 has been reported as an AEA-uptake inhibitor that shows various *in vivo* effects that are consistent with indirect cannabinoid CB<sub>1</sub> receptor activation by elevated AEA levels. However, the molecular target of WOBE437 is unknown. In this chapter, a photoaffinity-based approach was employed to identify the protein targets of WOBE437 in Neuro-2a cells. Surprisingly, WOBE437 increased AEA uptake and decreased endogenous NAE levels in Neuro-2a cells. Although the WOBE437-induced time-dependent decrease in endogenous AEA levels appears in keeping with the increased AEA uptake in Neuro-2a cells, it is unclear why the current results are in contrast to the previous findings of the laboratory of Dr. Gertsch.<sup>31</sup> Differences in the experimental protocol of AEA-uptake experiments or heterogeneity of Neuro-2a cells may be contributing factors. It should be noted that the positive control OMDM-1 did reduce AEA uptake in Neuro-2a cells under the same conditions. At the very least, this suggests that OMDM-1 and WOBE437 have different molecular modes of action, although both compounds are reported as AEA uptake inhibitors.

AfBPP using a WOBE437-based photoaffinity probe identified SCCPHD, VAT1 and FECH as WOBE437-interacting proteins in Neuro-2a cells. Competitive gel-based AfBPP demonstrated that SCCPHD and VAT1, but not FECH, could bind AEA preferentially over related lipids. Further genetic studies indicated, however, that SCCPDH and VAT1 were not responsible for the WOBE437-induced reduction in endogenous NAE levels in Neuro-2a cells. It remains to be investigated whether FECH is involved in this process. Regardless of the exact mechanism of action of WOBE437, the current study identified SCCPDH, VAT1 and FECH as off-targets of WOBE437, which may confound the interpretation of the biological effects obtained with this compound.

## Experimental procedures

### General

Lipids were purchased from Cayman Chemicals and stored as 10 mM ethanolic stocks under nitrogen at -80 °C, except glycerides, which were dissolved in acetonitrile. Inhibitors were purchased from Cayman Chemicals or Sigma Aldrich and stored as 10 mM DMSO stocks at -20 °C. FP-TAMRA was purchased from Thermo Fisher. MB064<sup>37</sup> and 3-(but-3-yn-1-yl)-3-(2-iodoethyl)-3*H*-diazirine<sup>38</sup> were prepared as previously reported in literature. All other reagents were purchased from Sigma Aldrich or Cayman Chemicals unless otherwise specified.

### Cloning

DNA oligos were purchased at Sigma Aldrich or Integrated DNA Technologies. Cloning reagents were from Thermo Fisher. Full-length cDNA encoding human and murine SCCPDH and VAT1, as well as human FECH was obtained from Source Bioscience. Expression constructs were generated by PCR amplification and restriction/ligation cloning into a pcDNA3.1 vector, in frame with a C-terminal FLAG tag. All plasmids were isolated from transformed XL10-Gold or DH10B competent cells (prepared using *E. coli* transformation buffer set, Zymo Research) using plasmid isolation kits following the supplier's protocol (Qiagen). All sequences were verified by Sanger sequencing (Macrogen).

### Cell culture

#### *General cell culture*

Neuro-2a and HEK-293-T cells were cultured at 37 °C under 7% CO<sub>2</sub> in DMEM (Sigma Aldrich, HEK-293-T: D6546, Neuro-2a: D1145) containing stable glutamine, 10% (v/v) New Born Calf Serum (Thermo Fisher) and penicillin and streptomycin (200 µg/mL each, Duchefa). Cells were passaged twice a week at 80-90% confluence by resuspension in fresh medium. Cell lines were purchased from ATCC and were tested regularly for mycoplasma contamination. Cultures were discarded after 2-3 months of use.

#### *Transfection*

SCCPDH/VAT1/FECH-overexpressing Neuro-2a or HEK-293-T cells were generated by seeding cells on 12-well plates (4.0x10<sup>4</sup> cells/cm<sup>2</sup>) 24 h prior to transfection. Culture medium was aspirated and replaced with 400 µL fresh medium. A mixture of polyethylenimine (PEI, Neuro-2a: 5:1 (m/m), HEK-293-T: 3:1 (m/m)) and plasmid DNA (0.625 µg/well) was prepared in serum-free culture medium (100 µL) and incubated for 15 min at rt. Transfection was performed by dropwise addition of the PEI/DNA mix to the cells. After 24 h, medium was refreshed. Cells were used 48 h post-transfection.

#### *Viability assay*

2.0x10<sup>5</sup> Neuro-2a cells were seeded in 500 µL medium on a 24-well plate 24 h prior. Then, 55 µL PBS supplemented with 5 mg/mL 3-(4,5-dimethylthiazol-2-yl)-2,5-diphenyltetrazolium bromide was added for 0.5 mg/mL final and the plate was incubated at 37 °C for 3 h. The medium was aspirated and the formed formazan crystals were dissolved in 200 µL DMSO by shaking the plates at 800 rpm for 5 min. Absorbance was measured at 450 nm in a CLARIOstar plate reader (BMG Labtech) and data was analyzed using Graphpad Prism 8.1.1.

#### *AEA uptake assay*

The uptake of AEA was measured in Neuro-2a cells (seeded in triplicate in 12-well plates) according to literature protocol with minor modifications.<sup>36</sup> Neuro-2a cells were pre-incubated in serum-free medium with OMDM-1 (40 µM) for 15 min or different concentrations of WOBE437 (0.1, 1, and 10 µM) or vehicle for 10 min by adding the substance directly to the incubation medium. Medium was aspirated and the cells were incubated with PBS at 37 °C containing AEA (400 nM) supplemented with [<sup>3</sup>H]AEA (30,000 cpm, ARC, St. Louis, MO, USA) for 15 min. PBS was then aspirated and the cells were washed three

## Chapter 6

times with PBS supplemented with 1% (w/v) BSA (1 mL) and resuspended in aq. NaOH (0.5 M, 0.5 mL) and measured in a scintillation counter. Control experiments were also carried out at 4 °C in order to subtract passive diffusion from active uptake.

### Photoaffinity-based protein profiling

#### *Gel-based AfBPP*

For gel-based profiling, transfected HEK-293-T or Neuro-2a (WT or KO) on 12-well plates were treated with probe as follows:

Growth medium was aspirated and a solution of indicated competitor (2X, 10  $\mu$ M final) or vehicle in serum-free DMEM supplemented with 0.1% (w/v) delipidated BSA (0.5 mL) was added and the cells were incubated for 30 min at 37 °C. Then, a solution of pac-WOBE (**3**, 2X, 100 nM final) in serum-free DMEM supplemented with 0.1% (w/v) delipidated BSA (0.5 mL) was added and the cells were incubated for 30 min at 37 °C. Medium was aspirated and replaced with 1 mL ice-cold DPBS and the cells were irradiated using a Caprobox™ (10 min, 4 °C, 350 nm, "UV") or exposed to ambient light (10 min, 4 °C, "No UV").

The cells were harvested by pipetting and pelleted by centrifugation (1,000 *g*, 10 min, 4 °C). The supernatant was removed and the cells were lysed by resuspension in lysis buffer (250 mM sucrose, 20 mM HEPES pH 7.5, 1 mM MgCl<sub>2</sub>, 1X protease inhibitor cocktail (Roche), 25 U/mL benzonase) and sonication in a bath sonicator (0 °C, 5 min). Protein concentration was measured by Qubit™ assay (Invitrogen) and the samples were adjusted to 1.5 mg/mL and a volume of 100  $\mu$ L, after which the samples were treated with 10.4  $\mu$ L click mix (5.5  $\mu$ L aq. 25 mM CuSO<sub>4</sub>, 3.25  $\mu$ L aq. 250 mM NaAsc, 1.1  $\mu$ L 25 mM THPTA in DMSO, 0.55  $\mu$ L 0.9 mM Cy5-N<sub>3</sub> in DMSO) and left at rt for 1 h. Samples were then quenched by addition of 4X Laemmli buffer, boiled (5 min, 95 °C) and resolved by SDS-PAGE (10% acrylamide gel,  $\pm$ 80 min, 180 V) along with protein marker (PageRuler™ Plus, Thermo Fisher). In-gel fluorescence was measured in the Cy3- and Cy5-channel (Chemidoc™ MP, Bio-Rad) and the gels were subsequently stained with Coomassie and imaged as a loading control for normalization of fluorescence intensity. Band intensities were quantified using Image Lab 6.0.1 (BioRad).

For VAT-1 western blot, part of the gel was stained with Coomassie and imaged for loading control. The rest of the gel was transferred to a 0.2  $\mu$ m polyvinylidene difluoride membrane by Trans-Blot Turbo™ Transfer system (Bio-Rad). Membranes were washed with TBS (50 mM Tris pH 7.5, 150 mM NaCl) and blocked with 5% (w/v) milk in TBS-T (50 mM Tris pH 7.5, 150 mM NaCl, 0.05% (w/v) Tween-20) for 1 h at rt. Membranes were then washed three times with TBS-T, followed by incubation with primary antibody in 5% (w/v) BSA in TBS-T (VAT1, PA5-43777, Thermo Fisher, 1:1,000, 1 h, rt). Membranes were then washed three times with TBS-T and incubated with secondary goat-anti-rabbit-HRP (sc-2030, Santa Cruz, 1:5,000 in 5% (w/v) milk in TBS-T, 1 h, rt), then washed three times with TBS-T and once with TBS before developing. Membranes were developed in luminol development solution (10 mL of 1.4 mM luminol in 100 mM Tris pH 8.8 + 100  $\mu$ L of 6.7 mM *p*-coumaric acid in DMSO + 3  $\mu$ L of 30% (v/v) H<sub>2</sub>O<sub>2</sub>) and chemiluminescence was detected on ChemiDoc™ MP (Bio-Rad) in the chemiluminescence channel and colorimetric channel for the protein marker. Images were processed using Image Lab 6.0.1 (BioRad).

#### *Chemical proteomics-based AfBPP*

Neuro-2a cells were plated on 6-well plates and grown to near confluency (90%). The supernatant was aspirated and serum-free DMEM supplemented with 0.1% (w/v) delipidated BSA (1 mL) and WOBE-437 or vehicle was added and the cells were incubated for 30 min at 37 °C. After this period, pac-WOBE (**3**) was added and the cells were incubated for 30 min at 37 °C. Subsequently, medium was aspirated and replaced with 1 mL ice-cold DPBS and the cells were irradiated using a Caprobox™ (10 min, 4 °C, 350 nm, "UV") or exposed to ambient light (10 min, 4 °C, "No UV"). The cells were harvested by pipetting and pelleted by centrifugation (1,000 *g*, 10 min, 4 °C). The supernatant was removed and the cells were lysed by resuspension in lysis buffer (250  $\mu$ L, 250 mM sucrose, 20 mM HEPES pH 7.5, 1 mM MgCl<sub>2</sub>,

1X protease inhibitor cocktail (Roche)) and sonication (Branson Sonifier probe sonicator, 10 x 2 s pulses, 10% amplitude). Protein concentration was measured by Qubit™ assay (Invitrogen) and the samples were adjusted using 50 mM HEPES pH 7.5 to a protein concentration of 1.0 mg/mL and a volume of 400  $\mu$ L. The pulldown experiment was performed as earlier described, with minor adjustments.<sup>39,45</sup> The lysates (400  $\mu$ L) were subjected to a click reaction with freshly prepared click mix (43.7  $\mu$ L per sample: 21.9  $\mu$ L aq. 25 mM CuSO<sub>4</sub>, 13  $\mu$ L aq. 250 mM NaAsc, 4.4  $\mu$ L 25 mM THPTA in DMSO, 4.4  $\mu$ L 2.25 mM biotin-N<sub>3</sub> in DMSO) at rt for 1 h. Proteins were precipitated by addition of HEPES buffer (50  $\mu$ L, 50 mM, pH 7.5), MeOH (666  $\mu$ L), CHCl<sub>3</sub> (166  $\mu$ L) and MilliQ (150  $\mu$ L), vortexing after each addition. After spinning down (1,500 *g*, 10 min) the upper and lower layer were aspirated and the protein pellet was resuspended in MeOH (600  $\mu$ L) by sonication (Branson Sonifier probe sonicator, 10 x 0.5 s pulses, 10% amplitude). The proteins were spun down (20,000 *g*, 5 min) and the MeOH was aspirated. The proteins were redissolved in 6 M urea (500  $\mu$ L) with 25 mM NH<sub>4</sub>HCO<sub>3</sub> for 15 min, followed by reduction (65 °C, 15 min, 800 rpm shaking) with DTT (5  $\mu$ L, 1 M). The samples were allowed to reach rt and proteins were alkylated (30 min) with IAA (40  $\mu$ L, 0.5 M) in the dark. 140  $\mu$ L SDS (10% w/v) was added and the samples were spun down (1,000 *g*, 5 min). They were transferred to 5 mL PBS containing 50  $\mu$ L avidin agarose resin (Pierce, 100  $\mu$ L of a 50% slurry, prewashed twice with 6 mL PBS + 0.5% SDS and once with 6 mL PBS) and incubated for 2 h while rotating. The beads were spun down (2,000 *g*, 2 min) and washed (3 x PBS + 0.5% SDS, 2 x PBS, 1 x MilliQ). The beads were resuspended in digestion buffer (250  $\mu$ L, 100 mM Tris pH 7.8, 100 mM NaCl, 1 mM CaCl<sub>2</sub>, 2% (v/v) acetonitrile, sequencing grade trypsin (Promega, 0.25  $\mu$ g)) and transferred to low-binding tubes (Sarstedt) and incubated while shaking overnight (16 h, 37 °C, 1,000 rpm). Trypsin was quenched with 12.5  $\mu$ L formic acid (LC-MS grade) and the beads were filtered off over a Bio-Spin column (BioRad, 400 *g*, 5 min), collecting the flow-through in a new 2 mL tube. Samples were added on C18 stagetips<sup>46</sup> (preconditioned with 50  $\mu$ L MeOH, then 50  $\mu$ L of 0.5% (v/v) formic acid in 80% (v/v) acetonitrile/MilliQ (solution B) and then 50  $\mu$ L 0.5% (v/v) formic acid in MilliQ (solution A) by centrifugation (600 *g*, 2 min)). The peptides were washed with solution A (100  $\mu$ L, 800 *g*, 3 min) and eluted into new low-binding tubes using solution B (100  $\mu$ L, 800 *g*, 3 min). Samples were concentrated using an Eppendorf speedvac (Eppendorf Concentrator Plus 5301) and redissolved in LC-MS solution (30  $\mu$ L per sample: 28.5  $\mu$ L MilliQ, 2.85  $\mu$ L acetonitrile, 0.095  $\mu$ L formic acid, 600 fmol yeast enolase peptide digest (Waters, 186002325)).

Samples were measured using a NanoACQUITY UPLC System coupled to a SYNAPT G2-Si high definition mass spectrometer (Waters). The peptides were separated using an analytical column (HSS-T3 C18 1.8  $\mu$ m, 75  $\mu$ m x 250 mm, Waters) with a concave gradient (5 to 40% acetonitrile in H<sub>2</sub>O with 0.1% formic acid). [Glu<sup>1</sup>]-fibrinopeptide B was used as lock mass. Mass spectra were acquired using the UDMS<sup>e</sup> method. The mass range was set from 50 to 2,000 Da with a scan time of 0.6 seconds in positive, resolution mode. The collision energy was set to 4 V in the trap cell for low-energy MS mode. For the elevated energy scan, the transfer cell collision energy was ramped using drift-time-specific collision energies. The lock mass is sampled every 30 seconds. For raw data processing, Progenesis QI for proteomics was used with the following parameters to search the murine proteome from Uniprot (Table S1).

**Table S1 | Parameters used for Progenesis QI.**

Parameter	Value
Lock mass <i>m/z</i> value	785.8426
Low energy threshold	150 counts
Elevated energy threshold	30 counts
Digest reagent	Trypsin
Missed cleavages	Max 2
Modifications	Fixed carbamidomethyl C, variable oxidation M
FDR less than	1%
Minimum fragments/peptide	2
Minimum fragments/protein	5
Minimum peptides/protein	1
Minimum peptide score for quantification	5.5
Identified ion charges for quantification	2/3/4/5/6/7 <sup>+</sup>

### Activity-based protein profiling

To perform comparative ABPP, 39  $\mu\text{L}$  of lysate (39  $\mu\text{g}$  protein) was mixed with 1  $\mu\text{L}$  of indicated compound (40X stock in DMSO) before probe addition. Final concentration of probes were 500 nM for FP-TAMRA and 2  $\mu\text{M}$  for MB064. The probes were incubated for 30 min at rt before quenching the reaction with 4X Laemmli buffer for 30 min at rt. Labelled proteins were resolved by SDS-PAGE (10% acrylamide gel,  $\pm 80$  min, 180 V) along with protein marker (PageRuler™ Plus, Thermo Fisher). In-gel fluorescence was measured in the Cy3- and Cy5-channel (Chemidoc™ MP, Bio-Rad) and the gels were subsequently stained with Coomassie and imaged as a loading control for normalization of fluorescence intensity. Band intensities were quantified using Image Lab 6.0.1 (BioRad).

### Lipidomics

A targeted analysis of 23 compounds, including endocannabinoids and related *N*-acylethanolamines (NAEs) and free fatty acids (Table S2), was measured using an Acquity UPLC I class binary solvent manager pump in conjugation with a tandem quadrupole mass spectrometer as mass analyzer (Waters Corporation). The separation was performed with an Acquity HSS T3 column (2.1  $\times$  100 mm, 1.8  $\mu\text{m}$ ) maintained at 45 °C. The aqueous mobile phase A consisted of 2 mM ammonium formate and 10 mM formic acid, and the organic mobile phase B was acetonitrile. The flow rate was set to 0.55 mL/min; initial gradient conditions were 55% B held for 2 min and linearly ramped to 100% B over 6 min and held for 2 min; after 10 s the system returned to initial conditions and held 2 min before next injection. Electrospray ionization-MS and a selective Multiple Reaction Mode (sMRM) was used for lipid quantification. Individually optimized MRM transitions using their synthetic standards for target compounds and internal standards are described in Table S2. Peak area integration was performed with MassLynx 4.1 software (Waters Corporation). The obtained peak areas of targets were corrected by appropriate internal standards. Calculated response ratios, determined as the peak area ratios of the target analyte to the peak area of the respective internal standard, were used to obtain absolute concentrations from their respective calibration curves. Concentrations were normalized to the amount of protein in the sample as determined by Bradford assay.

**Table S2 | LC-MS standards and internal standards for lipidomics analysis.** The target list includes fatty acids, endocannabinoids, *N*-acylethanolamines (NAEs) and deuterated labeled internal standards. The compound ID is the abbreviation of metabolite name along with number of carbon atoms and number of double bonds in the fatty acid chain of the molecule, respectively. All compounds are analyzed in positive mode except fatty acids in negative mode. Q1 and Q3 are optimized precursor ion and product ion respectively, expressed as m/z. DP and CE are declustering potential (V) and collision energy (V).

Standards					
Abbreviation	Metabolite	Q1	Q3	DP, CE	Polarity
<b>1 &amp; 2-AG (20:4)</b>	1-Arachidonoyl Glycerol	379.21	287.20	45, 10	+
<b>2-LG (18:2)</b>	2-Linoleoyl Glycerol	357.34	247.50	48, 10	+
<b>2-OG (18:1)</b>	2-Oleoyl Glycerol	357.34	247.50	40, 12	+
<b>AEA (20:4)</b>	Arachidonoyl Ethanolamide	348.40	62.02	35, 16	+
<b>DEA (22:4)</b>	Docosatetraenoyl Ethanolamide	376.38	61.92	55, 18	+
<b>DGLEA (18:3)</b>	Dihomo- $\gamma$ -Linolenoyl Ethanolamide	350.38	61.98	40, 14	+
<b>DHEA (22:6)</b>	Docosahexaenoyl Ethanolamide	372.38	62.01	50, 14	+
<b>EPEA (20:5)</b>	Eicosapentaenoyl Ethanolamide	346.34	61.98	36, 16	+
<b>LEA (18:2)</b>	Linoleoyl Ethanolamide	324.34	61.98	35, 14	+
<b>OEA (18:1)</b>	Oleoyl Ethanolamide	326.4	62.01	45, 16	+
<b>PDEA (15:0)</b>	Pentadecanoyl Ethanolamide	286.34	62.01	45, 12	+
<b>PEA (16:0)</b>	Palmitoyl Ethanolamide	300.34	61.98	42, 14	+
<b>POEA (16:1)</b>	Palmitoleoyl Ethanolamide	298.34	62.01	45, 14	+
<b>SEA (18:0)</b>	Stearoyl Ethanolamide	328.38	61.98	45, 16	+
<b>AA (20:4)</b>	Arachidonic Acid	302.28	259.30	-40, -12	-
<b>PA (FA 16:0)</b>	Palmitic Acid	255.33	237.24	-50, -20	-
<b>OA (FA 18:1)</b>	Oleic Acid	281.34	263.31	-50, -20	-
<b>LA (FA 18:2)</b>	Linoleic Acid	279.34	261.25	-64, -16	-
<b>GLA (FA 18:3)</b>	$\gamma$ -Linolenic Acid	277.30	58.00	-60, -20	-
<b>ETA (FA 20:3, (<math>\omega</math>-3))</b>	Eicosatrienoic Acid	305.28	306.09	-60, -18	-
<b>DGLA (FA 20:3, (<math>\omega</math>-6))</b>	Dihomo- $\gamma$ -Linolenic Acid (20:3)	305.28	306.03	-66, -18	-
<b>EPA (FA 20:5, (<math>\omega</math>-3))</b>	Eicosapentaenoic Acid	301.34	257.30	-60, -10	-
<b>DHA (FA 22:6, (<math>\omega</math>-3))</b>	Docosahexaenoic Acid	327.28	283.31	-60, -10	-
Internal standards					
Abbreviation	Metabolite	Q1	Q3	DP, CE	Polarity
<b>2-AG-d8 (20:4)</b>	2-Arachidonoyl Glycerol-d8	387.38	294.20	45, 10	+
<b>AEA-d8 (20:4)</b>	Arachidonoyl Ethanolamide-d8	356.38	62.79	35, 16	+
<b>DHEA-d4 (22:6)</b>	Docosahexaenoyl Ethanolamide-d4	376.38	66.01	50, 14	+
<b>LEA-d4 (18:2)</b>	Linoleoyl Ethanolamide-d4	328.34	66.01	35, 16	+
<b>OEA-d4 (18:1)</b>	Oleoyl Ethanolamide-d4	330.38	66.01	45, 16	+
<b>PEA-d5 (16:0)</b>	Palmitoyl Ethanolamide-d5	305.34	61.98	42, 16	+
<b>SEA-d3 (18:0)</b>	Stearoyl Ethanolamide-d3	331.38	61.91	45, 16	+
<b>EPEA-d4 (20:5)</b>	Eicosapentaenoyl Ethanolamide-d4	350.34	66.08	36, 18	+
<b>AA-d8 (20:4)</b>	Arachidonic Acid-d8	311.34	267.30	-40, -12	-
<b>PA (16:0)-d31</b>	Palmitic Acid-d31	286.50	266.37	-40, -22	-

### CRISPR/Cas9 KO generation

#### *Guide design & constructs*

Two sgRNAs, in early exons of the *Vat1* and *Sccpdh* genes, with high efficiency and specificity as predicted by CHOPCHOP v2 online web tool were selected.<sup>47</sup> Guides were cloned into the *BbsI* restriction site of plasmid px330-U6-Chimeric\_BB-CBh-hSpCas9 (a kind gift from Feng Zhang, Addgene plasmid #42230) as previously described.<sup>48,49</sup> Primers are annotated in Table S3.

#### *CRISPR/Cas9-mediated knockout population generation*

*Note: Neuro-2a cells display high level of heterogeneity upon clonal isolation.<sup>44</sup> To circumvent this issue, sequential transfections were used to generate a high efficiency knockout cell population.*

Neuro-2a cells were transfected sequentially (3 times within the course of 10 days) to yield populations with a high knockout efficiency. Cells were seeded at day 1, 4, and 7 and transfected at day 2, 5, and 8. Samples for T7E1 assays were harvested at day 4, 7, and 10 and after several weeks of culturing the cells. One day prior to the first transfection, Neuro-2a cells were seeded to a 6-well plate to reach 80% confluence at the time of transfection. Prior to transfection, culture medium was aspirated and 2 mL of fresh medium was added. A 5:1 (m/m) mixture of PEI (17.5 µg per well) and plasmid DNA (total 3.5 µg per well) was prepared in serum-free culture medium (250 µL each) and incubated (15 min, rt). Transfection was performed by dropwise addition of the PEI/DNA mixture to the cells. 24 h post-transfection the culture medium was refreshed. 48 h post-transfection a small amount of cells was harvested for analysis by T7E1 assay and ABPP, while the remainder was kept in culture under standard conditions for following transfections. After three transfection rounds, the cells were cultured according to standard protocol. Ampoules of knockdown populations were prepared (complete DMEM, 10% DMSO) and stored at -150 °C. Efficiency of knockdown was checked over time. Cells were discarded after 3 months of culture.

#### *T7E1 assay*

Genomic DNA was obtained by mixing 50 µL QuickExtract™ (Epicentre) with cell pellet (~10% of a well from a 6-well plate). The samples were incubated at 65 °C for 6 min, mixed by vortexing and incubated at 98 °C for 2 min. Genomic DNA extracts were diluted in sterile water and directly used in PCR reactions. Genomic PCR reactions were performed on 5 µL isolated genomic DNA extract using Phusion High-Fidelity DNA Polymerase (Thermo Fisher) in Phusion GC buffer Green (Thermo Fisher) in a final volume of 45 µL, primers are annotated in Table S3.

For the T7E1 assay, genomic PCR products (20 µL) were denatured and reannealed in a thermocycler using the following program: 5 min at 95 °C, 95 to 85 °C using a ramp rate of -2 °C/s, 85 °C to 25 °C using a ramp rate of -0.2 °C/s. Annealed PCR product (8.5 µL) was mixed with NEB2 buffer (1 µL) and T7 endonuclease I (5 U, 0.5 µL; New England Biolabs), followed by a 30 min incubation at 37 °C. Digested PCR products were analyzed using agarose gel electrophoresis with ethidium bromide staining. A sample without T7 endonuclease I was taken along as control. Agarose gels were analyzed using Image Lab 6.0.1 (BioRad).

**Table S3 | sgRNA targets, sgRNA oligos (top, bottom) and T7E1 primers (forward, reverse).**

sgRNA Target	Construct	Primer Sequences
<b><i>Vat1</i> – Exon 1</b>	1162	Top: CACCGTTCGCAGCCCCGACAGTCG Bottom: AAACCGACTGTCGGGGGCTGCGAAC Forward: TCAGGGTACCTATCAGTCACACGCACGTACAC Reverse: CCATGGGCCCGTAGTCGGTCGTACAGCCCTT
		<b>– Exon 2</b> 1163
<b><i>Scdph</i> – Exon 1</b>	1164	Top: CACCGAGGCGCCGAACACCACCAGG Bottom: AAACCCTGGTGGTGTTCGGCGCCTC Forward: TCAGGGTACCGCTTCAGGGGAACCAAGAG Reverse: CCATGGGCCCGCCGTGTTACCCAGTTTCTG
		<b>– Exon 2</b> 1165

### NAPE-PLD surrogate substrate-based fluorescence assay

The NAPE-PLD activity assay was performed according to a previously reported method with minor adjustments.<sup>50,51</sup> Purified recombinant MBP-tagged (N-terminal) and His<sub>6</sub>-tagged (C-terminal) human  $\Delta 47$ -NAPE-PLD from *Escherichia coli*, a kind gift from Dr. Piomelli, was diluted to 25 nM in assay buffer (50 mM Tris pH 7.5, 150 mM NaCl, 0.02% Triton X-100).<sup>52</sup> The substrate PED6 (Invitrogen, D23739, 1 mM stock in DMSO) was consecutively diluted in DMSO (5X) and in assay buffer (10X), to make a 20  $\mu$ M working solution. Inhibitor solutions (50X) were prepared in DMSO. The assay was performed in a dark 96-well plate (flat bottom, Greiner), in a final volume of 50  $\mu$ L. Inhibitor or DMSO was incubated with enzyme (2.5 nM final) for 30 min at 37 °C. Then, PED6 was added (2  $\mu$ M final) and the measurement was started immediately on a CLARIOstar plate reader (BMG Labtech) at 37 °C (excitation 474-490 nm, emission 510-550 nm), scanning every 2 min for 1 hour. Negative control wells containing no enzyme were used for background subtraction. The measurements were performed in n = 4.

### Statistical analysis

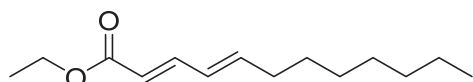
Unless otherwise noted, all replicates represent biological replicates and all data represent means  $\pm$  SEM. Statistical significance was determined using Student's t-tests (two-tailed, unpaired) or one-way ANOVA with Dunnett multiple comparisons correction. \*\*\* p < 0.001; \*\* p < 0.01; \* p < 0.05; n.s. if p > 0.05. All statistical analysis were conducted using Graphpad Prism 8.1.1 or Microsoft Excel.

## Synthesis

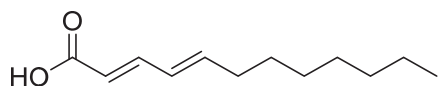
*General remarks*

Dry solvents were prepared by storage on activated 4 Å molecular sieves for at least 24 hours. The reactions were performed under an inert atmosphere of nitrogen gas unless stated otherwise. All reagents were purchased from Alfa Aesar, Sigma Aldrich/Merck or Acros and used without further purification. Flash column chromatography was performed using SiliCycle silica gel type SiliaFlash P60 (230-400 mesh). TLC analysis was performed on Merck silica gel 60/Kieselguhr F254, 0.25 mm. Compounds were visualized using KMnO<sub>4</sub> stain (K<sub>2</sub>CO<sub>3</sub> (40 g), KMnO<sub>4</sub> (6 g), and water (600 mL)).

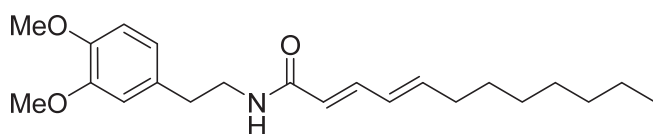
<sup>1</sup>H NMR and <sup>13</sup>C NMR spectra were recorded on a Bruker AV-400 (400 MHz) or AV-500 (500 MHz) spectrometer. Chemical shift values are reported in ppm relative to the tetramethylsilane signal for <sup>1</sup>H NMR ( $\delta = 0$  ppm) and relative to the solvent signal of CDCl<sub>3</sub> for <sup>13</sup>C NMR ( $\delta = 77.16$  ppm). Data are reported as follows: Chemical shifts ( $\delta$ ), multiplicity (s = singlet, d = doublet, dd = doublet of doublets, ddt = doublet of doublet of triplets, td = triplet of doublets, t = triplet, q = quartet, p = pentet, bs = broad singlet, m = multiplet), coupling constants *J* (Hz), and integration. High resolution mass spectra (HRMS) were recorded by direct injection on a q-TOF mass spectrometer (Synapt G2-SI) equipped with an electrospray ion source in positive mode with Leu-enkephalin (*m/z* = 556.2771) as an internal lock mass. The instrument was calibrated prior to measurement using the MS/MS spectrum of [Glu<sup>1</sup>]-fibrinopeptide B.

**Ethyl (2*E*,4*E*)-dodeca-2,4-dienoate (5)**

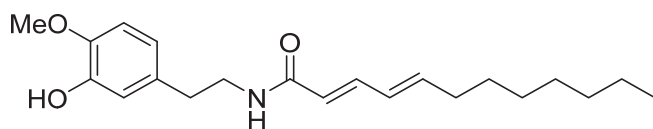
To a cooled (0 °C) suspension of sodium hydride (0.518 g, 12.94 mmol) in dry THF (30 mL) was added a solution of ethyl 2-(diethoxyphosphoryl)acetate (2.90 g, 12.94 mmol in dry THF (10 mL)) dropwise and the reaction was stirred for 10 min. It was then cooled to -78 °C and a solution of (*E*)-dec-2-enal (1.98 mL, 10.8 mmol) in dry THF (10 mL) was added dropwise and the reaction was allowed to reach rt overnight. The reaction was quenched with water (150 mL) and the mixture was extracted with EtOAc (2 x 150 mL). The combined organic layers were washed with brine (100 mL), dried over MgSO<sub>4</sub>, filtered and concentrated under reduced pressure. Purification of the residue by column chromatography (pentane/Et<sub>2</sub>O = pentane to 9:1) afforded the title compound as a clear oil (1.5281 g, 6.81 mmol, 63%). *R<sub>f</sub>* = 0.4 (pentane/Et<sub>2</sub>O = 19:1); <sup>1</sup>H NMR (400 MHz, CDCl<sub>3</sub>)  $\delta$  7.35 – 7.19 (m, 1H), 6.23 – 6.06 (m, 2H), 5.78 (d, *J* = 15.4 Hz, 1H), 4.20 (q, *J* = 7.1 Hz, 2H), 2.16 (q, *J* = 7.1 Hz, 2H), 1.48 – 1.38 (m, 2H), 1.38 – 1.19 (m, 11H), 0.88 (t, *J* = 6.7 Hz, 3H); <sup>13</sup>C NMR (101 MHz, CDCl<sub>3</sub>)  $\delta$  167.48, 145.27, 144.96, 128.44, 119.25, 60.30, 33.14, 31.91, 29.28, 29.24, 28.85, 22.78, 14.46, 14.23. Spectra were consistent with previously reported data.<sup>31</sup>

**(2*E*,4*E*)-dodeca-2,4-dienoic acid (6)**

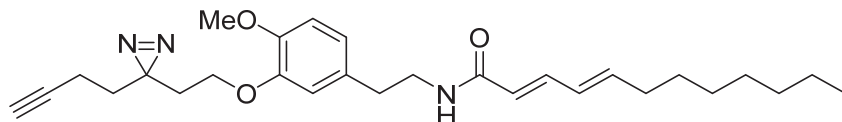
To a solution of ester **5** (1.514 g, 6.75 mmol) in MeOH (17 mL) was added 2 M aq. NaOH (6.75 mL, 13.50 mmol) and the reaction was stirred at 60 °C for 30 min. Solvent was removed under reduced pressure and the reaction was diluted with water (10 mL), washed with Et<sub>2</sub>O (20 mL), acidified with 1 M aq. HCl to pH <4 and extracted with EtOAc (2 x 20 mL). The combined organic layers were washed with brine (20 mL), dried over MgSO<sub>4</sub>, filtered and concentrated under reduced pressure to afford the title compound as an off-white solid (1.324 g, 6.75 mmol, quant.). *R<sub>f</sub>* = 0.6 (pentane/EtOAc = 1:1 + 0.5% AcOH); <sup>1</sup>H NMR (400 MHz, CDCl<sub>3</sub>)  $\delta$  7.40 – 7.30 (m, 1H), 6.23 – 6.16 (m, 2H), 5.78 (d, *J* = 15.3 Hz, 1H), 2.23 – 2.13 (m, 2H), 1.48 – 1.39 (m, 2H), 1.37 – 1.19 (m, 8H), 0.87 (t, *J* = 6.7 Hz, 3H); <sup>13</sup>C NMR (101 MHz, CDCl<sub>3</sub>)  $\delta$  172.81, 147.77, 146.56, 128.33, 118.27, 33.22, 31.91, 29.29, 29.24, 28.76, 22.78, 14.24. Spectra were consistent with previously reported data.<sup>31</sup>

**(2E,4E)-N-(3,4-dimethoxyphenethyl)dodeca-2,4-dienamide (WOBE437, 1)**

To a solution of carboxylic acid **6** (0.2500 g, 1.274 mmol) and 2-(3,4-dimethoxyphenyl)ethan-1-amine (0.254 g, 1.401 mmol) in DCM (2.5 mL) was added HOAt (0.087 g, 0.637 mmol) and EDC (0.293 g, 1.528 mmol) and the reaction was stirred for 45 min. Then, it was diluted with DCM (100 mL) and sat. aq. NaHCO<sub>3</sub> (100 mL). The layers were separated and the aq. layer was extracted with DCM (2 x 100 mL). The combined organic layers were dried over MgSO<sub>4</sub>, filtered and concentrated under reduced pressure. Purification of the residue by column chromatography (pentane/EtOAc = 1:4 to 1:1) afforded the title compound (WOBE437, **1**) as a white solid (0.3585 g, 0.997 mmol, 78%). R<sub>f</sub> = 0.5 (pentane/EtOAc = 1:1 + 0.5% AcOH); <sup>1</sup>H NMR (400 MHz, DMSO-*d*<sub>6</sub>) δ 8.00 (t, *J* = 5.7 Hz, 1H), 6.97 (dd, *J* = 15.1, 10.6 Hz, 1H), 6.85 (d, *J* = 8.2 Hz, 1H), 6.79 (d, *J* = 2.0 Hz, 1H), 6.70 (dd, *J* = 8.2, 2.0 Hz, 1H), 6.17 (dd, *J* = 15.2, 10.7 Hz, 1H), 6.06 (dt, *J* = 15.1, 6.7 Hz, 1H), 5.89 (d, *J* = 15.1 Hz, 1H), 3.72 (s, 3H), 3.70 (s, 3H), 3.33 – 3.28 (m, 2H), 2.66 (t, *J* = 7.3 Hz, 2H), 2.11 (q, *J* = 7.1 Hz, 2H), 1.43 – 1.32 (m, 2H), 1.32 – 1.17 (m, 8H), 0.89 – 0.82 (t, *J* = 6.7 Hz, 3H); <sup>13</sup>C NMR (101 MHz, DMSO) δ 165.21, 148.57, 147.20, 141.69, 139.12, 131.93, 128.60, 123.29, 120.42, 112.47, 111.83, 55.49, 55.34, 40.42, 34.72, 32.26, 31.25, 28.59, 28.53, 28.38, 22.10, 13.97. Spectra were consistent with previously reported data.<sup>31</sup>

**(2E,4E)-N-(3-hydroxy-4-methoxyphenethyl)dodeca-2,4-dienamide (7)**

To a cooled (0 °C) solution of 5-(2-aminoethyl)-2-methoxyphenol hydrochloride (0.0836 g, 0.408 mmol) in dry DMF (1.5 mL) was added carboxylic acid **6** (0.088 g, 0.449 mmol), EDC (0.094 g, 0.490 mmol), HOBT (0.066 g, 0.490 mmol) and Et<sub>3</sub>N (0.114 mL, 0.817 mmol) after which the reaction was allowed to reach rt. After 3 hours, the reaction was diluted with water (25 mL) and the mixture was extracted with Et<sub>2</sub>O (2 x 30 mL). The combined organic layers were washed with brine (4 x 10 mL), dried over Na<sub>2</sub>SO<sub>4</sub>, filtered and concentrated under reduced pressure. Purification of the residue by column chromatography (pentane/EtOAc/CHCl<sub>3</sub> = 4/1/2 + 0.5% AcOH to 2/1/1 + 0.5% AcOH) afforded the title compound as an off-white solid (0.0611 g, 0.177 mmol, 43%). R<sub>f</sub> = 0.5 (pentane/EtOAc/CHCl<sub>3</sub> = 2/2/1 + 0.5% AcOH); <sup>1</sup>H NMR (400 MHz, CDCl<sub>3</sub>) δ 7.19 (dd, *J* = 15.0, 10.0 Hz, 1H), 6.82 – 6.75 (m, 2H), 6.67 (dd, *J* = 8.1, 2.2 Hz, 1H), 6.12 – 6.03 (m, 2H), 5.68 (d, *J* = 15.0 Hz, 1H), 5.56 (bs, 1H), 3.87 (s, 3H), 3.56 (q, *J* = 6.6 Hz, 2H), 2.75 (t, *J* = 6.8 Hz, 2H), 2.17 – 2.12 (m, 2H), 1.47 – 1.35 (m, 2H), 1.35 – 1.21 (m, 8H), 0.88 (t, *J* = 6.4 Hz, 3H); <sup>13</sup>C NMR (101 MHz, CDCl<sub>3</sub>) δ 166.72, 145.82, 145.43, 143.74, 141.83, 132.19, 128.26, 121.47, 120.32, 115.01, 110.99, 56.12, 40.85, 35.09, 33.10, 31.90, 29.26, 29.23, 28.90, 22.77, 14.22. Spectra were consistent with previously reported data.<sup>31</sup>

**(2E,4E)-N-(3-(2-(3-(but-3-yn-1-yl)-3H-diazirin-3-yl)ethoxy)-4-methoxyphenethyl)dodeca-2,4-dienamide (pac-WOBE, 3)**

A solution of phenol **7** (16.8 mg, 0.049 mmol), 3-(but-3-yn-1-yl)-3-(2-iodoethyl)-3*H*-diazirine **8** (19.3 mg, 0.078 mmol) and K<sub>2</sub>CO<sub>3</sub> (13.4 mg, 0.097 mmol) in dry DMF (0.5 mL) was purged with N<sub>2</sub> and stirred at 60 °C overnight. The mixture was quenched with water (4 mL), extracted with Et<sub>2</sub>O (3 x 5 mL), dried over Na<sub>2</sub>SO<sub>4</sub>, filtered and concentrated under reduced pressure. Phenol **7** and the title compound were separated by column chromatography (MeOH/DCM = 1:1,000 to 1:100) and the recovered phenol **7** was dissolved in dry DMF (0.5 mL) with 3-(but-3-yn-1-yl)-3-(2-iodoethyl)-3*H*-diazirine **8** (19.3 mg, 0.078 mmol) and K<sub>2</sub>CO<sub>3</sub> (13.4 mg, 0.097 mmol), purged with N<sub>2</sub> and stirred at 60 °C overnight. The mixture was quenched with water (4 mL), extracted with Et<sub>2</sub>O (3 x 5 mL), dried over Na<sub>2</sub>SO<sub>4</sub> and concentrated under reduced pressure. It was combined with previously isolated title compound and purified with

## Chapter 6

column chromatography twice (pentane/EtOAc = 9:1 to 2:1 followed by MeOH/DCM = 1:1,000 to 1:100) to afford the title compound (pac-WOBE, **3**) as a white solid (0.0065 g, 0.014 mmol, 29%).  $R_f = 0.7$  (pentane/EtOAc = 1:1 + 0.5% AcOH);  $^1\text{H}$  NMR (500 MHz,  $\text{CDCl}_3$ )  $\delta$  7.18 (dd,  $J = 15.0, 9.7$  Hz, 1H), 6.82 (d,  $J = 8.2$  Hz, 1H), 6.76 (dd,  $J = 8.1, 2.0$  Hz, 1H), 6.71 (d,  $J = 2.0$  Hz, 1H), 6.17 – 6.02 (m, 2H), 5.68 (d,  $J = 15.0$  Hz, 1H), 5.43 (bs, 1H), 3.89 – 3.84 (m, 5H), 3.57 (q,  $J = 6.7$  Hz, 2H), 2.78 (t,  $J = 6.9$  Hz, 2H), 2.14 (q,  $J = 6.9$  Hz, 2H), 2.09 (td,  $J = 7.6, 2.6$  Hz, 2H), 1.98 (t,  $J = 2.7$  Hz, 1H), 1.89 (t,  $J = 6.4$  Hz, 2H), 1.76 (t,  $J = 7.6$  Hz, 2H), 1.44 – 1.37 (m, 2H), 1.28 (m, 8H), 0.88 (t,  $J = 6.9$  Hz, 3H);  $^{13}\text{C}$  NMR (126 MHz,  $\text{CDCl}_3$ )  $\delta$  166.45, 148.51, 148.22, 143.63, 141.67, 131.67, 128.30, 121.70, 121.63, 114.55, 112.36, 83.06, 69.20, 63.96, 56.26, 40.90, 35.31, 33.28, 33.11, 32.85, 31.92, 29.29, 29.25, 28.95, 26.86, 22.78, 14.23, 13.45. HRMS: Calculated for  $[\text{C}_{28}\text{H}_{39}\text{N}_3\text{O}_3 + \text{H}]^+$  466.3064, found 466.3073.

## Supplementary data

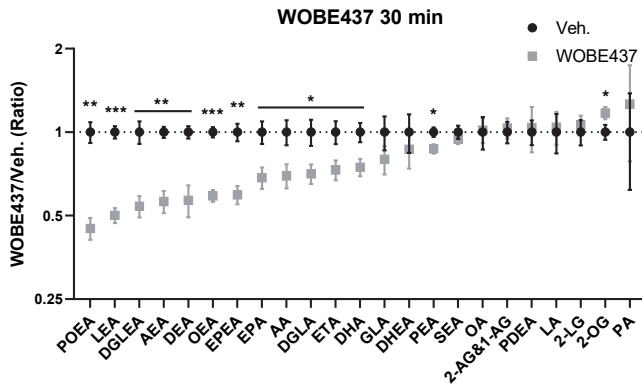


**Figure S1 | Lipid levels of Neuro-2a cells after 30 min of WOBE437 treatment corresponding to Figure 3.** Neuro-2a cells were treated with 10  $\mu$ M WOBE437 or vehicle and harvested after 30 min to be analyzed by MS-based lipidomics. Lipid levels are relative to vehicle-treated control. Data represent means  $\pm$  SEM (n = 4), t-test with Benjamini-Hochberg correction: \* q < 0.05, \*\* q < 0.01, \*\*\* q < 0.001.

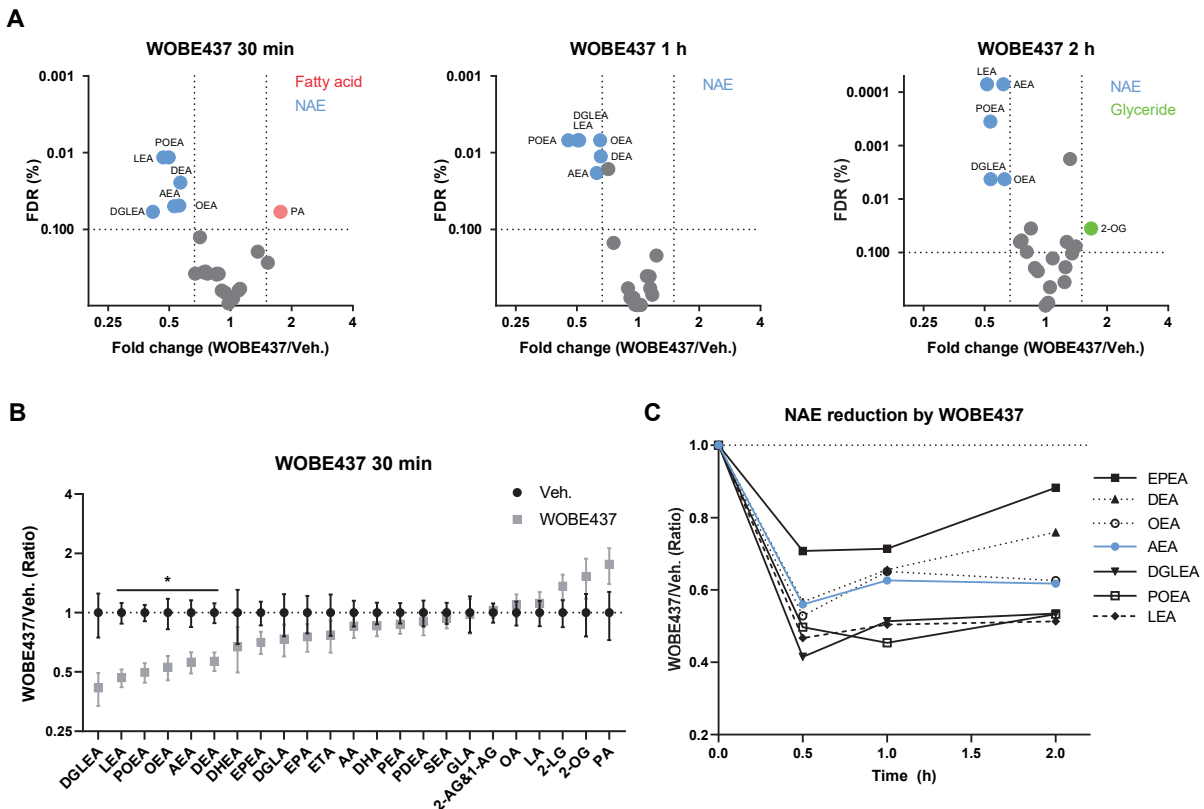


**Figure S2 | NAE disruption of WOBE437 on different passage of Neuro-2a.** Neuro-2a cells kept in culture for over 2.5 months were treated with 10  $\mu$ M WOBE437 or vehicle and harvested at the indicated time points to be analyzed by MS-based lipidomics. **(A)** Lipidomic data are presented as a volcano plot and lipids with a fold-change threshold of  $\geq 1.50$  or  $\leq 0.67$  and a Benjamini-Hochberg false-discovery rate (FDR)  $\leq 10\%$  are represented by colored circles indicating lipid class (n = 4). **(B)** All ratios of measured lipids after 30 min of WOBE437 treatment. Lipid levels are relative to vehicle-treated control. Data represent means  $\pm$  SEM (n = 4), t-test with Benjamini-Hochberg correction: \* q < 0.05. **(C)** Selected NAE ratios over time after WOBE437 incubation.

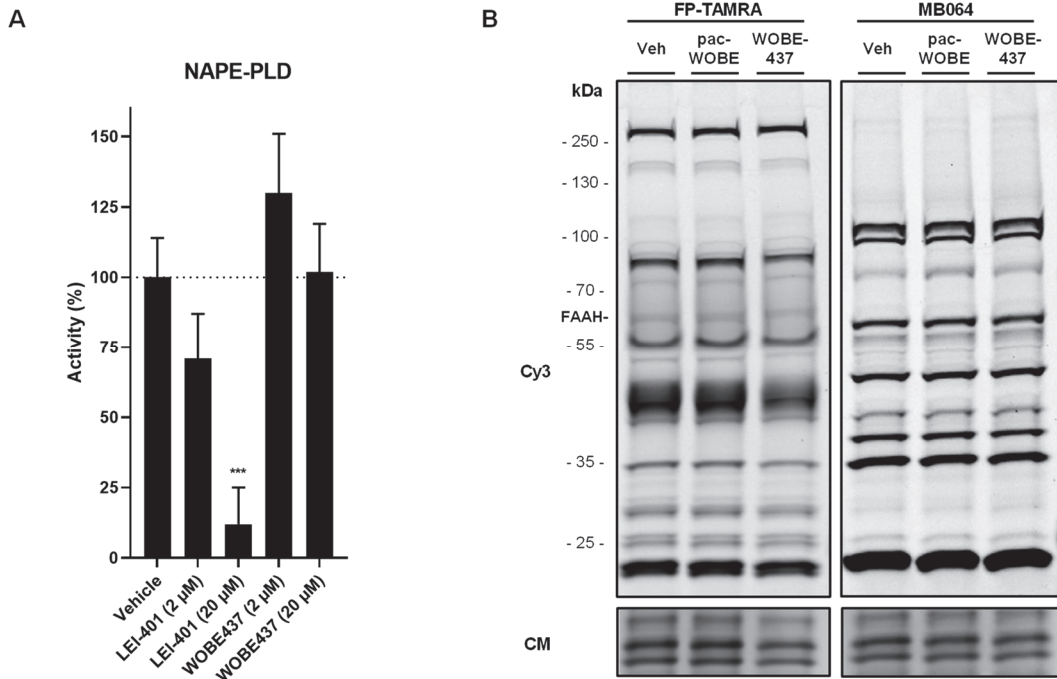


**Figure S3 | NAPE-PLD activity assay and serine hydrolase ABPP. (A)** Activity of recombinant human NAPE-PLD as tested in a PED6 surrogate substrate assay using LEI-401 as positive control.<sup>51</sup> Data represent means  $\pm$  SD (n = 4), one-way ANOVA with Dunnett’s multiple comparisons correction: \*\*\* p < 0.001 in comparison to vehicle-treated control (Dotted line). **(B)** Neuro-2a lysate was preincubated with 10  $\mu$ M of indicated compound or vehicle followed by FP-TAMRA or MB064 after which the labeled proteins were resolved by SDS-PAGE and in-gel fluorescence was detected. Coomassie served as a protein loading control.

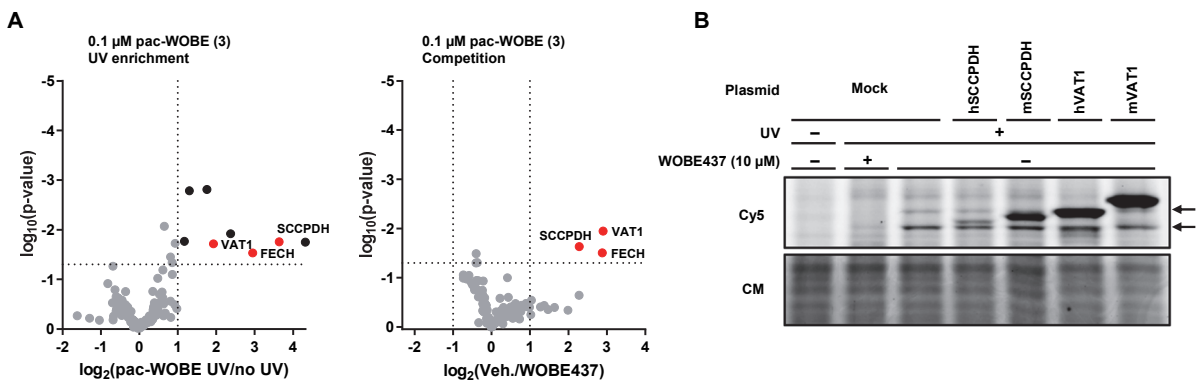


**Figure S4 | Pulldown and overexpression of pac-WOBE (3) targets in Neuro-2a. (A)** Volcano plots of pulldown experiment using 0.1  $\mu$ M pac-WOBE (3) and 10  $\mu$ M WOBE437 corresponding to Figure 5, Table S4. **(B)** Neuro-2a cells were transfected with indicated plasmid and treated with 10  $\mu$ M WOBE437 or vehicle and subsequently with 0.1  $\mu$ M pac-WOBE (3), irradiated, lysed and proteomes were conjugated to Cy5-N<sub>3</sub> using CuAAC chemistry and analyzed by SDS-PAGE and in-gel fluorescence scanning. Coomassie served as a protein loading control. Arrows indicate endogenous WOBE437 targets.

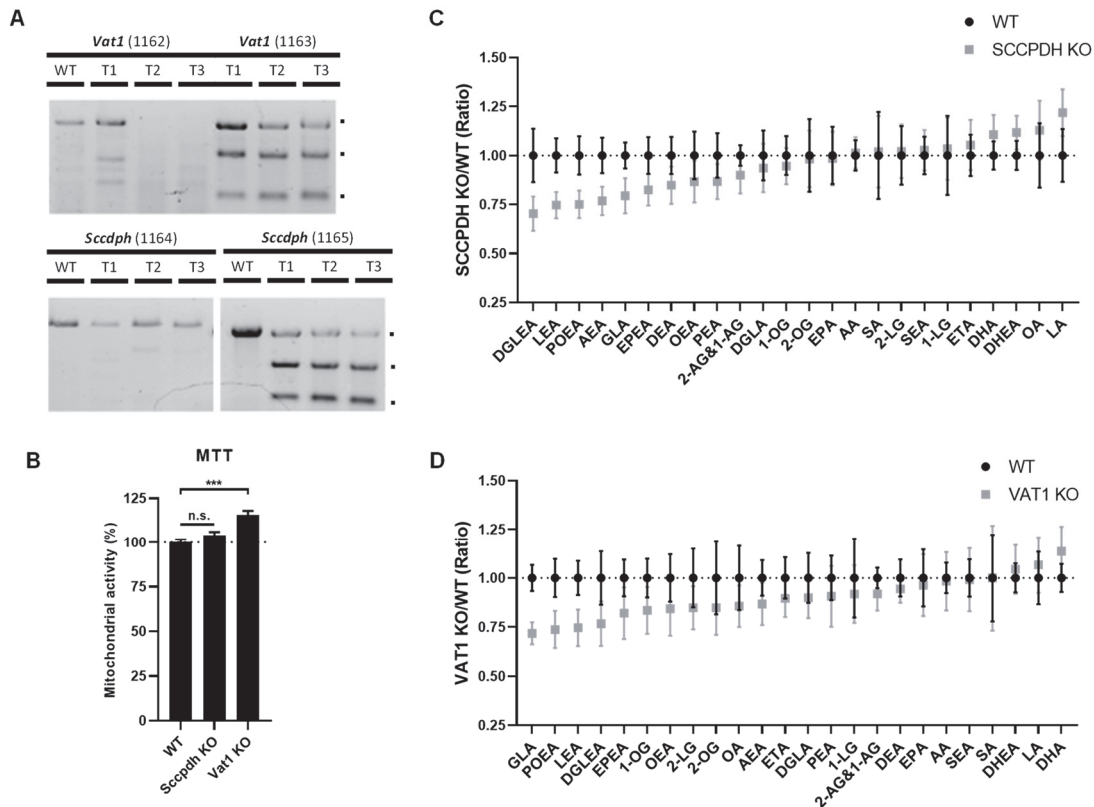


**Figure S5 | Characterization of CRISPR/Cas9-mediated knockouts in Neuro-2a.** (A) Knockout populations were generated by three sequential transfections (T1-T3) with Cas9 and two different separate guides for each target. Knockdown efficiency was determined by a T7E1 assay on genomic DNA, which was analyzed after each round of transfection for *Vat1* and *Scdph* knockouts. (B)  $2.0 \times 10^5$  Neuro-2a cells were plated and after 24 h checked for mitochondrial activity by MTT assay. Values shown are mean mitochondrial activity relative to WT Neuro-2a  $\pm$  SEM (n = 6), one-way ANOVA with Dunnett's multiple comparisons correction: \*\*\* p < 0.001 in comparison to WT. (C) SCCPDH KO and (D) VAT1 KO lipid ratios corresponding to Figure 6. Lipid levels relative to WT Neuro-2a. Data represent means  $\pm$  SEM (n = 4), t-test with Benjamini-Hochberg correction: not significant.

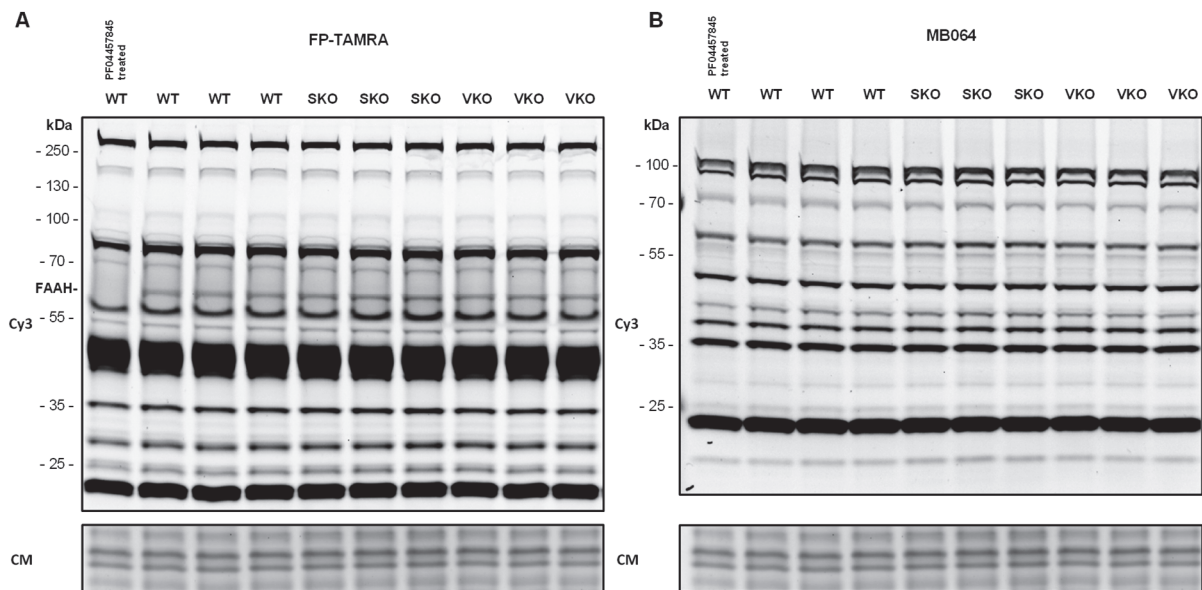


**Figure S6 | SCCPDH (SKO) or VAT1 (VKO) knockdown does not affect serine hydrolases labeled by FP-TAMRA or MB064.** Neuro-2a serine hydrolases were labeled with (A) FP-TAMRA or (B) MB064 in triplicate and the labeled proteins were resolved by SDS-PAGE and in-gel fluorescence was detected. Coomassie served as a protein loading control.

**Table S4 | All proteins significantly UV-enriched by 1  $\mu$ M pac-WOBE (3).**

Gene name	Unique peptides	Description	1 $\mu$ M pac-WOBE (3)				0.1 $\mu$ M pac-WOBE (3)			
			UV/noUV	p-value	Veh/WOBE	p-value	UV/noUV	p-value	Veh/WOBE	p-value
TOMM22	3	Mitochondrial import receptor subunit TOM22 homolog	$\infty$	0.0108	1.02	0.9209	995	0.0176	1.62	0.4054
SRPRB	5	Signal recognition particle receptor subunit beta	83.6	0.0354	0.56	0.2953	3.26	0.0832	1.00	0.9937
TIMM17B	3	Mitochondrial import inner membrane translocase subunit Tim17-B	72.3	0.0165	0.75	0.3197	5.18	0.0119	0.85	0.4630
<b>FECH</b>	<b>20</b>	<b>Ferroxidase mitochondrial</b>	<b>68.9</b>	<b>0.0000</b>	<b>8.62</b>	<b>0.0000</b>	<b>7.71</b>	<b>0.0293</b>	<b>7.37</b>	<b>0.0310</b>
<b>VAT1</b>	<b>12</b>	<b>Synaptic vesicle membrane protein VAT-1 homolog</b>	<b>53.8</b>	<b>0.0272</b>	<b>5.44</b>	<b>0.0379</b>	<b>3.80</b>	<b>0.0191</b>	<b>7.48</b>	<b>0.0112</b>
HSD17B12	16	Very-long-chain 3-oxoacyl-CoA reductase	47.6	0.0084	1.01	0.9378	7.96	0.0794	1.42	0.3886
LSS	14	Lanosterol synthase	44.6	0.0210	1.13	0.5565	3.53	0.1759	1.40	0.5063
CYB5B	2	Cytochrome b5 type B	36.2	0.0246	0.79	0.6025	$\infty$	0.3910	176.1	0.3932
<b>SCCPDH</b>	<b>10</b>	<b>Saccharopine dehydrogenase-like oxidoreductase</b>	<b>30.5</b>	<b>0.0208</b>	<b>2.91</b>	<b>0.0308</b>	<b>12.5</b>	<b>0.0175</b>	<b>4.87</b>	<b>0.0230</b>
EMB	2	Embigin	21.1	0.0042	0.67	0.2760	2.25	0.1379	1.20	0.5608
TMEM199	2	Transmembrane protein 199	20.5	0.0008	0.69	0.2993	2.16	0.3167	1.80	0.3856
PHB2	2	Prohibitin-2	18.6	0.0073	1.10	0.6037	4.83	0.3220	1.46	0.6590
PCYOX1	5	Prenylcysteine oxidase	17.5	0.0091	0.99	0.9770	2.46	0.0016	1.16	0.2582
TMEM33	7	Transmembrane protein 33	16.2	0.0082	0.83	0.3693	3.39	0.0015	0.92	0.6712
SGPL1	3	Sphingosine-1-phosphate lyase 1	15.8	0.0005	1.01	0.9108	1.41	0.4232	1.23	0.4534
EPHX1	3	Epoxide hydrolase 1	8.61	0.0178	0.74	0.4935	1.57	0.0084	0.94	0.6247
BSG	6	Basigin	8.08	0.0186	0.57	0.3377	1.81	0.0456	0.96	0.7915
IAP	17	IgE-binding protein	7.51	0.0018	0.59	0.2785	1.53	0.0647	0.75	0.1173
LRRC59	4	Leucine-rich repeat-containing protein 59	7.17	0.0081	0.80	0.5381	2.75	0.0655	1.19	0.4612
LBR	2	Lamin-B receptor	6.94	0.0045	0.66	0.3621	1.81	0.0792	0.94	0.6368
SEC61A1	2	Protein transport protein Sec61 subunit alpha isoform 1	6.88	0.0082	0.64	0.3321	2.04	0.1468	0.85	0.1786
TMX1	3	Thioredoxin-related transmembrane protein 1	6.69	0.0032	0.80	0.3149	3.17	0.0614	1.18	0.5139
RPN1	14	Dolichyl-diphosphooligosaccharide-protein glycosyltransferase subunit 1	6.31	0.0423	0.70	0.3664	1.75	0.0351	0.93	0.4492
VDAC1	12	Voltage-dependent anion-selective channel protein 1	6.00	0.0018	0.77	0.4955	1.53	0.2356	1.33	0.0992
ATP2A2	12	Sarcoplasmic/endoplasmic reticulum calcium ATPase 2	4.79	0.0115	0.71	0.2963	1.27	0.1740	0.96	0.7365
VDAC2	5	Voltage-dependent anion-selective channel protein 2	4.78	0.0086	0.73	0.4201	2.25	0.0170	0.95	0.7329
DHRS1	2	Dehydrogenase/reductase SDR family member 1	4.76	0.0059	1.46	0.1048	1.24	0.6531	2.06	0.2849
STT3A	5	Dolichyl-diphosphooligosaccharide-protein glycosyltransferase subunit STT3A	4.54	0.0049	0.79	0.3747	1.50	0.1787	0.77	0.0488
PDIA3	2	Protein disulfide-isomerase A3	4.54	0.0003	1.23	0.4045	3.01	0.3298	2.59	0.3620
RTN4	2	Reticulon-4	4.34	0.0439	0.88	0.4041	3.90	0.2232	1.51	0.5317
SLC25A3	8	Phosphate carrier protein mitochondrial	3.86	0.0224	0.81	0.5785	1.91	0.0187	0.96	0.6610
HSPA9	3	Stress-70 protein mitochondrial	3.63	0.0403	1.84	0.2066	4.36	0.2304	4.85	0.2252
VDAC3	5	Voltage-dependent anion-selective channel protein 3	3.39	0.0251	0.96	0.8860	1.39	0.0945	0.99	0.9584
RAB1A	2	Ras-related protein Rab-1A	3.14	0.0403	0.84	0.6040	1.29	0.3577	1.02	0.9054
ATP5F1B	6	ATP synthase subunit beta mitochondrial	2.81	0.0072	0.94	0.7622	2.76	0.3547	2.42	0.3870
HNRNPA1	2	Heterogeneous nuclear ribonucleoprotein A1	2.17	0.0329	1.71	0.2078	2.78	0.2948	1.98	0.3933
HSPD1	2	60 kDa heat shock protein mitochondrial	2.17	0.0465	0.90	0.7459	1.55	0.3124	1.01	0.9522
PRPH	5	Peripherin	2.10	0.0129	1.19	0.1558	1.75	0.2736	1.49	0.3740
UBA52	6	Ubiquitin-60S ribosomal protein L40	2.09	0.0108	0.72	0.2937	1.12	0.7069	0.96	0.7858

## References

- (1) Pacher, P.; Bátkai, S.; Kunos, G. The Endocannabinoid System as an Emerging Target of Pharmacotherapy. *Pharmacol. Rev.* **2006**, *58* (3), 389–462.
- (2) Mechoulam, R.; Parker, L. A. The Endocannabinoid System and the Brain. *Annu. Rev. Psychol.* **2013**, *64* (1), 21–47.
- (3) Centonze, D.; Finazzi-Agrò, A.; Bernardi, G.; Maccarrone, M. The Endocannabinoid System in Targeting Inflammatory Neurodegenerative Diseases. *Trends Pharmacol. Sci.* **2007**, *28* (4), 180–187.
- (4) Skaper, S. D.; Di Marzo, V. Endocannabinoids in Nervous System Health and Disease: The Big Picture in a Nutshell. *Philos. Trans. R. Soc. B Biol. Sci.* **2012**, *367* (1607), 3193–3200.
- (5) Klein, T. W. Cannabinoid-Based Drugs as Anti-Inflammatory Therapeutics. *Nat. Rev. Immunol.* **2005**, *5* (5), 400–411.
- (6) Pacher Pál; Mukhopadhyay Partha; Mohanraj Rajesh; Godlewski Grzegorz; Bátkai Sándor; Kunos George. Modulation of the Endocannabinoid System in Cardiovascular Disease. *Hypertension* **2008**, *52* (4), 601–607.
- (7) Steffens, S.; Pacher, P. Targeting Cannabinoid Receptor CB2 in Cardiovascular Disorders: Promises and Controversies. *Br. J. Pharmacol.* **2012**, *167* (2), 313–323.
- (8) Montecucco, F.; Di Marzo, V. At the Heart of the Matter: The Endocannabinoid System in Cardiovascular Function and Dysfunction. *Trends Pharmacol. Sci.* **2012**, *33* (6), 331–340.
- (9) Guindon, J.; Hohmann, A. G. Cannabinoid CB2 Receptors: A Therapeutic Target for the Treatment of Inflammatory and Neuropathic Pain. *Br. J. Pharmacol.* **2008**, *153* (2), 319–334.
- (10) Guindon, J.; Hohmann, A. G. The Endocannabinoid System and Pain. *CNS Neurol. Disord. Drug Targets* **2009**, *8* (6), 403–421.
- (11) Hillard, C. J.; Weinlander, K. M.; Stuhr, K. L. Contributions of Endocannabinoid Signaling to Psychiatric Disorders in Humans: Genetic and Biochemical Evidence. *Neuroscience* **2012**, *204*, 207–229.
- (12) Pacher, P.; Mechoulam, R. Is Lipid Signaling through Cannabinoid 2 Receptors Part of a Protective System? *Prog. Lipid Res.* **2011**, *50* (2), 193–211.
- (13) Pacher, P.; Kunos, G. Modulating the Endocannabinoid System in Human Health and Disease – Successes and Failures. *FEBS J.* **2013**, *280* (9), 1918–1943.
- (14) Marzo, V. D.; Bifulco, M.; Petrocellis, L. D. The Endocannabinoid System and Its Therapeutic Exploitation. *Nat. Rev. Drug Discov.* **2004**, *3* (9), 771–784.
- (15) Sandberg, A.; Fowler, C. J. Measurement of Saturable and Non-Saturable Components of Anandamide Uptake into P19 Embryonic Carcinoma Cells in the Presence of Fatty Acid-Free Bovine Serum Albumin. *Chem. Phys. Lipids* **2005**, *134* (2), 131–139.
- (16) Beltramo, M.; Stella, N.; Calignano, A.; Lin, S. Y.; Makriyannis, A.; Piomelli, D. Functional Role of High-Affinity Anandamide Transport, as Revealed by Selective Inhibition. *Science* **1997**, *277* (5329), 1094–1097.
- (17) Petrocellis, L. D.; Bisogno, T.; Davis, J. B.; Pertwee, R. G.; Marzo, V. D. Overlap between the Ligand Recognition Properties of the Anandamide Transporter and the VR1 Vanilloid Receptor: Inhibitors of Anandamide Uptake with Negligible Capsaicin-like Activity. *FEBS Lett.* **2000**, *483* (1), 52–56.
- (18) López-Rodríguez, M. L.; Viso, A.; Ortega-Gutiérrez, S.; Fowler, C. J.; Tiger, G.; de Lago, E.; Fernández-Ruiz, J.; Ramos, J. A. Design, Synthesis, and Biological Evaluation of New Inhibitors of the Endocannabinoid Uptake: Comparison with Effects on Fatty Acid Amidohydrolase. *J. Med. Chem.* **2003**, *46* (8), 1512–1522.
- (19) Ortar, G.; Ligresti, A.; De Petrocellis, L.; Morera, E.; Di Marzo, V. Novel Selective and Metabolically Stable Inhibitors of Anandamide Cellular Uptake. *Biochem. Pharmacol.* **2003**, *65* (9), 1473–1481.
- (20) Maccarrone, M. Metabolism of the Endocannabinoid Anandamide: Open Questions after 25 Years. *Front. Mol. Neurosci.* **2017**, *10*.
- (21) Deutsch, D. G. A Personal Retrospective: Elevating Anandamide (AEA) by Targeting Fatty Acid Amide Hydrolase (FAAH) and the Fatty Acid Binding Proteins (FABPs). *Front. Pharmacol.* **2016**, *7*.
- (22) Fowler, C. J. Anandamide Uptake Explained? *Trends Pharmacol. Sci.* **2012**, *33* (4), 181–185.
- (23) Nicolussi, S.; Gertsch, J. Chapter Fourteen - Endocannabinoid Transport Revisited. In *Vitamins & Hormones*; Litwack, G., Ed.; Hormones and Transport Systems; Academic Press, 2015; Vol. 98, pp 441–485.
- (24) Glaser, S. T.; Kaczocha, M.; Deutsch, D. G. Anandamide Transport: A Critical Review. *Life Sci.* **2005**, *77* (14), 1584–1604.
- (25) Glaser, S. T.; Abumrad, N. A.; Fatade, F.; Kaczocha, M.; Studholme, K. M.; Deutsch, D. G. Evidence against the Presence of an Anandamide Transporter. *Proc. Natl. Acad. Sci.* **2003**, *100* (7), 4269–4274.
- (26) Kaczocha, M.; Hermann, A.; Glaser, S. T.; Bojesen, I. N.; Deutsch, D. G. Anandamide Uptake Is Consistent with Rate-Limited Diffusion and Is Regulated by the Degree of Its Hydrolysis by Fatty Acid Amide Hydrolase. *J. Biol. Chem.* **2006**, *281* (14), 9066–9075.
- (27) Cravatt, B. F.; Giang, D. K.; Mayfield, S. P.; Boger, D. L.; Lerner, R. A.; Gilula, N. B. Molecular Characterization of an Enzyme That Degrades Neuromodulatory Fatty-Acid Amides. *Nature* **1996**, *384* (6604), 83–87.
- (28) Kaczocha, M.; Glaser, S. T.; Deutsch, D. G. Identification of Intracellular Carriers for the Endocannabinoid Anandamide. *Proc. Natl. Acad. Sci.* **2009**, *106* (15), 6375–6380.

- (29) Oddi, S.; Fezza, F.; Pasquariello, N.; D'Agostino, A.; Catanzaro, G.; De Simone, C.; Rapino, C.; Finazzi-Agrò, A.; Maccarrone, M. Molecular Identification of Albumin and Hsp70 as Cytosolic Anandamide-Binding Proteins. *Chem. Biol.* **2009**, *16* (6), 624–632.
- (30) Fu, J.; Bottegoni, G.; Sasso, O.; Bertorelli, R.; Rocchia, W.; Masetti, M.; Guijarro, A.; Lodola, A.; Armirotti, A.; Garau, G.; Bandiera, T.; Reggiani, A.; Mor, M.; Cavalli, A.; Piomelli, D. A Catalytically Silent FAAH-1 Variant Drives Anandamide Transport in Neurons. *Nat. Neurosci.* **2012**, *15* (1), 64–69.
- (31) Chicca, A.; Nicolussi, S.; Bartholomäus, R.; Blunder, M.; Rey, A. A.; Petrucci, V.; Reynoso-Moreno, I. del C.; Viveros-Paredes, J. M.; Gens, M. D.; Lutz, B.; Schiöth, H. B.; Soeberdt, M.; Abels, C.; Charles, R.-P.; Altmann, K.-H.; Gertsch, J. Chemical Probes to Potently and Selectively Inhibit Endocannabinoid Cellular Reuptake. *Proc. Natl. Acad. Sci.* **2017**, *114* (25), E5006–E5015.
- (32) Reynoso-Moreno, I.; Chicca, A.; Flores-Soto, M. E.; Viveros-Paredes, J. M.; Gertsch, J. The Endocannabinoid Reuptake Inhibitor WOBE437 Is Orally Bioavailable and Exerts Indirect Polypharmacological Effects via Different Endocannabinoid Receptors. *Front. Mol. Neurosci.* **2018**, *11*.
- (33) Maccarrone, M.; Fiorucci, L.; Erba, F.; Bari, M.; Finazzi-Agrò, A.; Ascoli, F. Human Mast Cells Take up and Hydrolyze Anandamide under the Control of 5-Lipoxygenase and Do Not Express Cannabinoid Receptors. *FEBS Lett.* **2000**, *468* (2–3), 176–180.
- (34) Lapinsky, D. J.; Johnson, D. S. Recent Developments and Applications of Clickable Photoprobes in Medicinal Chemistry and Chemical Biology. *Future Med. Chem.* **2015**, *7* (16), 2143–2171.
- (35) Hein, J. E.; Fokin, V. V. Copper-Catalyzed Azide-Alkyne Cycloaddition (CuAAC) and beyond: New Reactivity of Copper(I) Acetylides. *Chemical Society Reviews*. 2010, pp 1302–1315.
- (36) Fezza, F.; Oddi, S.; Tommaso, M. D.; Simone, C. D.; Rapino, C.; Pasquariello, N.; Dainese, E.; Finazzi-Agrò, A.; Maccarrone, M. Characterization of Biotin-Anandamide, a Novel Tool for the Visualization of Anandamide Accumulation. *J. Lipid Res.* **2008**, *49* (6), 1216–1223.
- (37) Baggelaar, M. P.; Janssen, F. J.; van Esbroeck, A. C. M.; den Dulk, H.; Allarà, M.; Hoogendoorn, S.; McGuire, R.; Florea, B. I.; Meeuwenoord, N.; van den Elst, H.; van der Marel, G. A.; Brouwer, J.; Di Marzo, V.; Overkleeft, H. S.; van der Stelt, M. Development of an Activity-Based Probe and In Silico Design Reveal Highly Selective Inhibitors for Diacylglycerol Lipase- $\alpha$  in Brain. *Angew. Chem. Int. Ed.* **2013**, *52* (46), 12081–12085.
- (38) Li, Z.; Hao, P.; Li, L.; Tan, C. Y. J.; Cheng, X.; Chen, G. Y. J.; Sze, S. K.; Shen, H.-M.; Yao, S. Q. Design and Synthesis of Minimalist Terminal Alkyne-Containing Diazirine Photo-Crosslinkers and Their Incorporation into Kinase Inhibitors for Cell- and Tissue-Based Proteome Profiling. *Angew. Chem.* **2013**, *125* (33), 8713–8718.
- (39) van Rooden, E. J.; Florea, B. I.; Deng, H.; Baggelaar, M. P.; van Esbroeck, A. C. M.; Zhou, J.; Overkleeft, H. S.; van der Stelt, M. Mapping *in Vivo* Target Interaction Profiles of Covalent Inhibitors Using Chemical Proteomics with Label-Free Quantification. *Nat. Protoc.* **2018**, *13* (4), 752–767.
- (40) Klaeger, S.; Gohlke, B.; Perrin, J.; Gupta, V.; Heinzlmeir, S.; Helm, D.; Qiao, H.; Bergamini, G.; Handa, H.; Savitski, M. M.; Bantscheff, M.; Médard, G.; Preissner, R.; Kuster, B. Chemical Proteomics Reveals Ferrochelatase as a Common Off-Target of Kinase Inhibitors. *ACS Chem. Biol.* **2016**, *11* (5), 1245–1254.
- (41) Koenders, S. T. A.; Gagstein, B.; van der Stelt, M. Opportunities for Lipid-Based Probes in the Field of Immunology. In *Activity-Based Protein Profiling*; Cravatt, B. F., Hsu, K.-L., Weerapana, E., Eds.; Current Topics in Microbiology and Immunology; Springer International Publishing: Cham, 2019; pp 283–319.
- (42) Junker, M.; Rapoport, T. A. Involvement of VAT-1 in Phosphatidylserine Transfer from the Endoplasmic Reticulum to Mitochondria. *Traffic* **2015**, *16* (12), 1306–1317.
- (43) Faugaret, D.; Chouinard, F. C.; Harbour, D.; El azreq, M.-A.; Bourgoin, S. G. An Essential Role for Phospholipase D in the Recruitment of Vesicle Amine Transport Protein-1 to Membranes in Human Neutrophils. *Biochem. Pharmacol.* **2011**, *81* (1), 144–156.
- (44) Van Esbroeck, A. C. M.; Kantae, V.; Di, X.; van der Wel, T.; den Dulk, H.; Stevens, A. F.; Singh, S.; Bakker, A. T.; Florea, B. I.; Stella, N.; Overkleeft, H. S.; Hankemeier, T.; van der Stelt, M. Identification of  $\alpha,\beta$ -Hydrolase Domain Containing Protein 6 as a Diacylglycerol Lipase in Neuro-2a Cells. *Front. Mol. Neurosci.* **2019**, *12*, 286.
- (45) Soethoudt, M.; Stolze, S. C.; Westphal, M. V.; van Stralen, L.; Martella, A.; van Rooden, E. J.; Guba, W.; Varga, Z. V.; Deng, H.; van Kasteren, S. I.; Grether, U.; IJzerman, A. P.; Pacher, P.; Carreira, E. M.; Overkleeft, H. S.; Ioan-Facsinay, A.; Heitman, L. H.; van der Stelt, M. Selective Photoaffinity Probe That Enables Assessment of Cannabinoid CB2 Receptor Expression and Ligand Engagement in Human Cells. *J. Am. Chem. Soc.* **2018**, *140* (19), 6067–6075.
- (46) Rappsilber, J.; Mann, M.; Ishihama, Y. Protocol for Micro-Purification, Enrichment, Pre-Fractionation and Storage of Peptides for Proteomics Using StageTips. *Nat. Protoc.* **2007**, *2* (8), 1896–1906.
- (47) Labun, K.; Montague, T. G.; Gagnon, J. A.; Thyme, S. B.; Valen, E. CHOPCHOP v2: A Web Tool for the next Generation of CRISPR Genome Engineering. *Nucleic Acids Res.* **2016**, *44*, 272–276.
- (48) Cong, L.; Ran, F. A.; Cox, D.; Lin, S.; Barretto, R.; Habib, N.; Hsu, P. D.; Wu, X.; Jiang, W.; Marraffini, L. A.; Zhang, F. Multiplex Genome Engineering Using CRISPR/Cas System. *Science* **2013**, *339* (February), 819–824.
- (49) Ran, F. A.; Hsu, P. D.; Wright, J.; Agarwala, V.; Scott, D. A.; Zhang, F. Genome Engineering Using the CRISPR-Cas9 System. *Nat. Protoc.* **2013**, *8* (11), 2281–2308.

- (50) Peppard, J. V.; Mehdi, S.; Li, Z.; Duguid, M. S. ASSAY METHODS FOR IDENTIFYING AGENTS THAT MODIFY THE ACTIVITY OF NAPE-PLD OR Abh4. US20100143937A1, June 10, 2010.
- (51) Mock, E. D.; Mustafa, M.; Gunduz-Cinar, O.; Cinar, R.; Petrie, G. N.; Kantae, V.; Di, X.; Ogasawara, D.; Varga, Z. V.; Paloczi, J.; Miliano, C.; Donvito, G.; van Esbroeck, A. C. M.; van der Gracht, A. M. F.; Kotsogianni, I.; Park, J. K.; Martella, A.; van der Wel, T.; Soethoudt, M.; Jiang, M.; Wendel, T. J.; Janssen, A. P. A.; Bakker, A. T.; Donovan, C. M.; Castillo, L. I.; Florea, B. I.; Wat, J.; van den Hurk, H.; Wittwer, M.; Grether, U.; Holmes, A.; van Boeckel, C. A. A.; Hankemeier, T.; Cravatt, B. F.; Buczynski, M. W.; Hill, M. N.; Pacher, P.; Lichtman, A. H.; van der Stelt, M. Discovery of a NAPE-PLD Inhibitor That Modulates Emotional Behavior in Mice. *Nat. Chem. Biol.* **2020**, 1–9.
- (52) Piomelli, D.; Magotti, P.; Bauer, I.; Igarashi, M.; Babagoli, M.; Marotta, R.; Garau, G. Structure of Human N -Acylphosphatidylethanolamine-Hydrolyzing Phospholipase D: Regulation of Fatty Acid Ethanolamide Biosynthesis by Bile Acids. *Structure* **2015**, *23* (3), 598–604.

